Thermo-mechanical properties of high strength concrete reinforced with nano-micro fibers under fire conditions

Submitted by

Muhammad Talal Afzal

Fall 2017-MS Structural Engineering

00000203030

MASTERS IN STRUCTURAL ENGINEERING

MS Thesis Advisor:

Dr. Rao Arsalan Khushnood

NUST Institute of Civil Engineering (NICE)

School of Civil and Environmental Engineering (SCEE)

National University of Sciences and Technology (NUST)

Islamabad, Pakistan (2019)

This is to certify that

Thesis titled

"Thermo-mechanical properties of high strength concrete reinforced with nano-micro fibers under fire conditions"

Submitted by

Muhammad Talal Afzal

Fall 2017-MS Structural Engineering

00000203030

Has been accepted towards the partial fulfillment

of

the requirements for the award of degree of

Master of Science in Structural Engineering

_____

Dr. Rao Arsalan Khushnood
Assistant Professor
NUST Institute of Civil Engineering (NICE)
School of Civil and Environmental Engineering (SCEE)
National University of Sciences and Technology (NUST),
Islamabad, Pakistan

THESIS ACCEPTANCE CERTIFICATE

Certified that final copy of MS thesis written by **Mr. Muhammad Talal Afzal,** Registration No. **(00000203030),** of MS Structure 2017 Batch (NICE) has been vetted by undersigned, found completed in all respects as per NUST Statutes/Regulations, is free of plagiarism, errors, and mistakes and is accepted as partial fulfillment for award of MS/MPhil degree. It is further certified that necessary amendments as pointed out by GEC members of the scholar have been incorporated in the said thesis.

Signature_____

Name of Supervisor Dr.Rao Arsalan Khushnood

Date: _____

Signature (HoD)_____

Date:_____

Signature (Dean/Principal)_____

Date:_____

DEDICATED

TO

MY PARENTS &

THEIR GRANDSON

SYED ABDULLAH SHAMIM

ACKNOWLEDGEMENTS

ABSTRACT

Carbon nano fibers (CNFs) and basalt fibers (BFs) were added into high strength concrete (HSC) to evaluate the fire resilience of incumbent matrix. The mechanical performance was evaluated by conducting material property tests namely compressive strength, tensile strength, stress–strain response, elastic modulus, compressive toughness and mass loss in the temperature range of $23^{o}C$ to $800^{o}C$. Heating rate of $5^{o}C$/min was employed to expose the concrete cylindrical samples to targeted temperatures. Advanced techniques such as scanning electron microscopy (SEM) have been used for micro and nano forensics while the internal structure damage on exposure to fire was analyzed by ultrasonic pulse velocity (UPV) in macro-phase. The test results revealed better retention in mechanical and physical properties of high strength concrete containing CNFs and BFs. Mathematical relationships based on statistical analysis have been proposed for predicting mechanical, durability and energy related properties of HSC modified with varying percentages of CNFs and BFs at elevated temperatures.

TABLE OF CONTENTS

LIST OF FIGURES

LIST OF TABLES

INTRODUCTION

1.1   General

Concrete is one of the most extensively used materials in the construction industry owing to its exceptional strength, durability and vast availability of ingredients [1]. In recent years, driven by the growing demand for high-rise buildings, normal strength concrete (NSC) has been sidelined, as it was not able to fulfill performance demands. Hence in order to design smaller cross-sections and higher permissible stresses, high strength concrete (HSC) was developed. As a consequence, utilization of HSC has grown incrementally over the past couple of decades [2]. HSC offers high mechanical strength i.e. compressive and tensile [2] durability against chemical attack [3] lower permeability [4]. This is due to a compact microstructure which develops as result of secondary cementing mechanism [5], filler effect of constituents and lower porosity [6].

However, studies reveal that the performance of high strength concrete when subjected to fire conditions is poor [7, 8]. HSC experiences undesirable chemical changes and thermal cracking at elevated temperatures which rapidly compromises its structural use [9]. Explosive spalling occurs due to the vaporization of water present in the pores. This pore pressure applies immense tensile stresses to inner micro core of concrete, which is weak in tension and gives way to this pressure in the form of excessive cracking [10]. Scaling of concrete from the external surface occurs when this pore pressure surpasses the concrete's tensile strength. With the elevation in temperature tensile strength decreases, thus putting concrete to a higher risk of spalling [1]. In addition to that, thermal stresses growth because of thermal inertia is the other reason of spalling[11]. The distribution of heat in the concrete core is lower than the outer layer. The outer layers of concrete are exposed to excessive heat and the transfer to inner layers is slow because of higher specific heat and lower thermal conductivity of concrete [12]. This process delays overall heat transfer to the inner layers of concrete leading to the development of thermal inertia. The heat gradient increase as a result of thermal inertia, induces thermal stresses which are tensile in nature. Subsequently, these stresses crack the matrix and the accumulation of these cracks causes spalling. So in order to make concrete potent against cracking and spalling, crack bridging and thermally efficient materials are often sought after.

Recently research and development in field of nanotechnology has made its way into building materials. Nanotechnology deals with matter with tolerances under 100nm and manipulates it at molecular level. New multifunctional high performance mixes have been developed. A lot of nano-modifiers are available that can be employed to achieve these new improved cementitious matrices, these include nano-particles (0D), nano-fibres (1D) and nanofoils (2D) [13] shown in Figure 1 [14]. Among these carbon nano-modifiers outmuscle all in terms of higher elastic modulus, strength, and resistance against corrosion. Graphite nano-particles when used in cementitious matrices improve mechanical performance in terms of self-sensing ability, enhanced tensile, compressive and flexural strength.
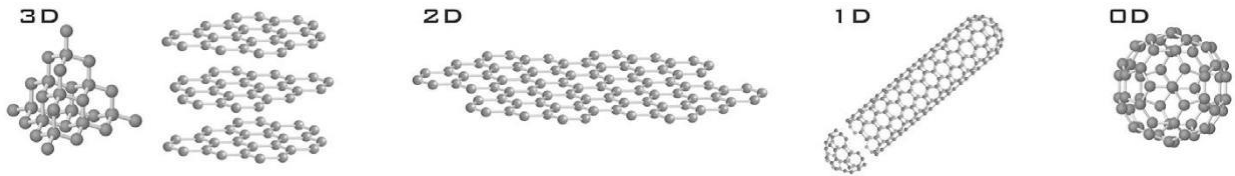
Figure 1: Left to right, 3D graphite and diamond, 2D graphene, 1D nanotube, 0D fullerene [14]
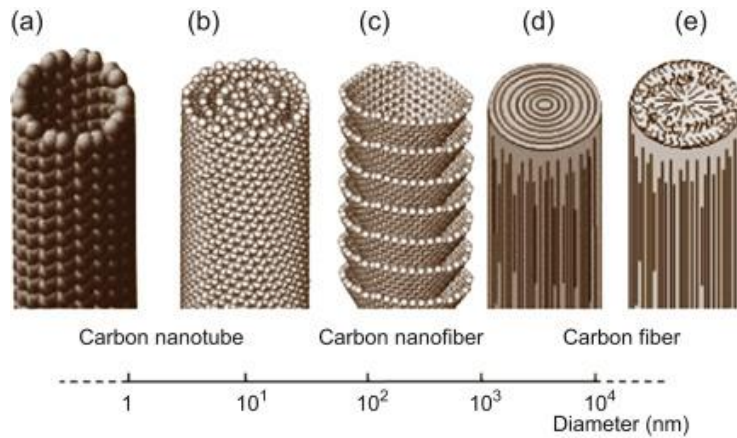
Figure 2: Diametric range for carbon fibers

Carbon nanofibers (CNFs) offer improvements similar to CNTs in terms of enhanced tensile strength, flexural strength and crack resistance [15, 16]. CNFs have crack bridging capability at nano level, and have higher bonding ability with cement products [17]. Studies show that CNFs enhance ductility, proportion of high density calcium silicate hydrate gel, fracture toughness and modulus of elasticity and which gets reflected in higher mechanical strength [17-19]. Carbon nano fibers possess high thermal and electrical conductivities, high stiffness, specific strength, tensile

2

modulus, corrosion and chemical resistance, which makes them suitable to be intruded as reinforcement to develop superior cementitious matrices [20-22]. CNFs have higher strength/weight ratio as compared to steel [23]. Similarly, CNFs give better performance compared to CNTs because of higher aspect ratio, which can arrest the nano-cracks more effectively [24]. In addition to that, by providing an anchor across CNFs can restrain the crack at nano-level and can delay its propagation. Fiber spacing is reduced due to nano scale diameter of CNFs that should theoretically restrain the formation and further growth of micro-cracks at initial level. CNFs have 100 times lower production cost than CNTs yet offers similar improvements in mechanical properties, microstructural refinement and other multifunctional properties for concrete [23]. In addition to that, physical configuration of CNFs offers numerous exposed edges along the surface, which in turn concocts potential sites of interfaces for hydration products to grow [25]. Sanchez et.al reported that CNFs are thermally stable and have higher heat resistance at elevated temperatures as compared to MWCNTs [26]. The aforementioned properties inspired us to evaluate the fire performance of concrete modified with CNFs.

Currently, numerous organic and inorganic fibers are available in construction market, however many of them either lack durability or structural strength or are extremely costly for use in moderate loadings. In present times, basalt fiber (BF) is the demanding fiber that is being used in construction industry. Because of novelty of basalt fiber it is extruded from inorganic basalt rock in temperature between 1460 °C to 1500 °C [27] and have recently gained popularity in structural applications owing to its considerable mechanical strength, high modulus, high chemical resistance, thermal stability, extended operating temperature range (−200 °C to 600 °C), non-combustible characteristics [28, 29] environmental friendliness, higher impact load capacity, and fire with less poisonous fumes and commercial availability [30].

Tensile strength of BF is higher compared to E-glass fiber, BF has higher strain at failure compared to carbon fiber (CF). In addition to that it has excellent resistance against impact load, chemical attack and creates less poisonous fumes in fire [31]. Adding economical cost of BF to its properties , this makes basalt fiber an appropriate alternative for steel, glass and carbon fibers in many construction works [32, 33]. For building structures, when adequate structural properties and enhanced fire resistance are all together required, cementitious composites reinforced with BF can be a better replacement to conventional matrices reinforced with fiber as when tested under 600°C

merely BF maintained its 90% of strength plus volumetric integrity than glass and carbon fibers [33]. The manufacturing process of BF is analogous to that of glass fiber, but with less energy consumed and no additives, that makes it inexpensive compared to GF and CF [34-36]. Additional benefits such as higher heat resistance, modulus, better endurance against chemical attack, exceptional interfacial shear strength and commercial availability, enable basalt fiber a good replacement to GF or CF [37].

Figure 3: Chopped basalt fiber

Concrete generally has low thermal conductivity ranging from 1.4 - 3.6 W/m°K [38]. While CNF's thermal conductivity is well above 3000 W/m°K at 23°C which surpasses that of diamond. While on the other hand basalt fiber (BF) is a thermally resistive fiber. So it would be interesting to see how a concrete containing CNFs and BFs will fare against elevated temperatures. Material properties of these nano and micro-modified composites have been well explored and detailed specifications have been updated in standards for concrete structures at ambient temperatures. However there is no reliable data yet published considering elevated temperature properties of these reinforced composites.

1.2 Research objectives

- To study thermal properties of high strength concrete reinforced with nano-micro fibers at elevated temperatures.
- To investigate mechanical and microstructural properties of high strength concrete reinforced with nano-micro fibers at elevated temperatures.
- To introduce mathematical relationships for the studied formulations exposed to elevated temperatures.

1.3   Research Tasks

To accomplish research objectives following tasks are performed

- Literature review
- Test set up which include furnace, splitting tensile test assembly, protective steel assembly
- Perform high temperature tests
- Evaluate and analyze experimental results
- Conclusions and recommendations

1.4   Research significance

The crack bridging and strengthening nature of CNFs in HSC under fire condition has not been identified. Most research on cement composites reinforced with carbon nano fibers to date has concentrated on the macroscopic properties but limited research has been conducted on the nanoscale mechanical properties, which are believed to highly influence the properties of materials. Thus an investigational methodology to identify the behavior of CNFs modified HSC at elevated temperatures has been designed which will yield novel understandings by witnessing behavioral variations in the thermo-mechanical and internal microstructural properties of HSC intruded with these carbon nano-fibers (CNFs) at elevated temperatures. Similarly, behavior of basalt fiber (BF) as a thermally resistive fiber in high strength concrete at elevated temperatures has been reported scarcely. Nonetheless, most research on cementitious and concrete composites reinforced with basalt fibers to date has concentrated on the mechanical properties but limited research has been conducted on the elevated temperature properties, which are believed to highly influence the properties of HSC such as strength, stiffness, durability, fracture behavior and residual behavior under fire conditions. The aim of this study is to investigate the elevated temperature thermal, mechanical and microstructural properties of HSC reinforced with BF& CNF under residual conditions. Qualitative microstructural study of morphological changes of heat treated specimens is also performed using scanning electron microscopy (SEM). The test data obtained experimental work will be used to formulate simplified mathematical equations, which will act as predictor and response factors in computer aided design and analysis.

1.5 Thesis outline

The research undertaken to address the aforementioned objectives is presented in five chapters. Chapter 1 outlines the behavior of HSC when exposed to elevated temperatures, research objectives and research significance has been discussed.

Chapter 2 describes literature review in detail. A brief literature review about properties of CNFs and BFs in general and when used in cementitious matrices has been provided. Elevated temperature performance of HSC has been discussed in detail, in addition to that test methods (residual) has been discussed.

Chapter 3 deals with the test setup. It explains which types of equipment used to evaluate mechanical properties. Furthermore it presents an overview of the test procedure which describes the ways and methods to determine mechanical properties.

Chapter 4 provides evaluation, analysis and discussion for results of material property tests. Results of thermal and mechanical.

Chapter 5 consist of the research conclusions and further recommendations

LITERATURE REVIEW

2.1   General

This chapter comprises of brief introduction about carbon nano fibers (CNFs) and basalt fibers (BFs), their production and usage in cementitious matrices. Properties of BFs and CNFs at ambient temperature have been discussed and literature on high strength concrete properties at elevated temperature has been discussed. Concrete is one of the most extensively used construction material due to its excellent performance in terms of high compressive strength, higher modulus of elasticity, ease of preparation, water tightness, resistance to corrosive agents, superior fire ratings and so on. From the day construction industry was introduced to concrete, there have been gradual developments in the properties of concrete. Compressive Strength is a direct indicator of the performance quality of concrete i.e. a concrete having greater compressive strength would be having greater modulus of elasticity, greater tensile strength, lower permeability and hence it would have higher durability. Most of the properties of concrete have a direct relationship with its compressive strength. There has been a gradual development in the compressive strength of concrete due to the advancements in material technology. Since the introduction of superplasticizers (SP) or high range water reducers (HRWRs), the use of HSC has become very common. HSC offers a number of advantages in terms of superior durability and economy. In current construction practice, use of HSC in the columns of high-rise buildings has become a complementary practice because it results in space-saving and economy due to reduced cross sections. Concrete structures in service may be subjected to higher temperatures in the event of fire. There are numerous studies on performance of concrete under elevated temperatures. Results have shown that, despite of excellent performance of HSC in all other scenarios, its performance under elevated temperatures is poor compared with NSC.

2.2   Nano Materials

The word "nano" comes from a Greek origin, meaning dwarf. Carbon atoms can arrange themselves in various geometric forms to make allotropes of completely different properties [39]. Nano materials should have at least one dimension in nanometer. Nano materials show different

physical and chemical properties than macro-scale material because of change in crystal and surface electronic structure [40].

2.3 Carbon-based cementitious nanocomposites

Studies on carbon-based cementitious nano composites started back in 1990's. Carbon nano tube (CNT) and carbon black (CB) were the two-carbon based nano-particles that were used at that time. CNT has two types, one is single walled carbon nano tube (SWCNT) having diameter of 0.75-3nm and length of 1-50um, other is multi walled carbon nano tube (MWCNT) having diameter of 2–30nm and length of 0.1–50um [41]. SWCNT has only one layer of graphene and MWCNT has multiple layers of graphene (single layer of two-dimensional carbon atoms bonded to form hexagonal lattice is called graphene) [42].

2.4 Carbon Nanofibers (CNFs)

Carbon nanofibers are carbon-based nano-material that are obtained from graphite. CNF has conical shaped dimensional structure composed of graphene layers having thickness in nanometer and diameter in the range of submicron to 100um. Because of higher aspect ratio and larger surface area, these nano fibers show good mechanical properties and also make conductive networks in composite materials. Typical structure difference of CNF as compared to CNT is represented in Figure 4.
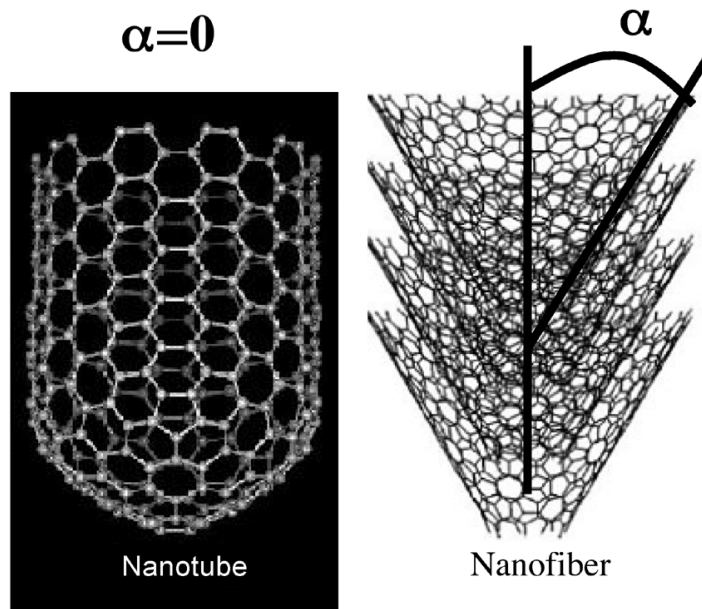
Figure 4: Difference between carbon nano tube and carbon nano fiber

2.5 Applications of Carbon Nanofibers

A lot of effort is being put to expand the novel application of this versatile material in diverse fields. The main focus of nanotechnology these days is in the sector of materials science, electronics, energy and medicine but quite recently nano-materials have entered the field of construction industry as well. By modifying the cementitious composites CNFs can play a significant role in construction industry. Extraordinary material properties of CNFs like high elasticity and strength can make the cementitious composites superior over conventional composites. CNFs has a wider range of application in construction industry, building materials, medicines, batteries, capacitors, membranes etc. Figure 5 shows numbers of applications of CNFs in various fields of sciences.
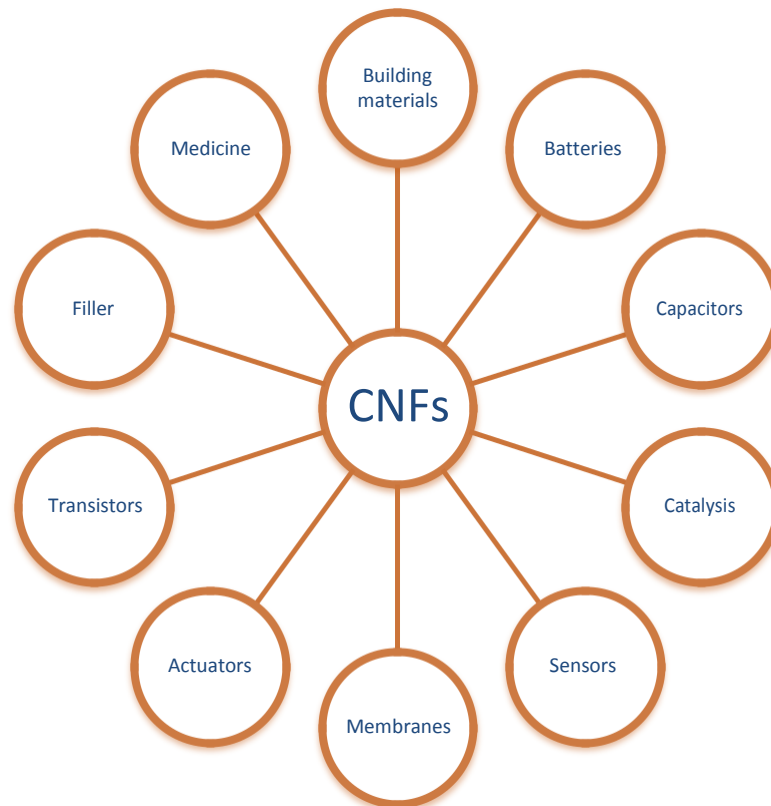
Figure 5: Applications of CNFs

2.6 Properties of Carbon Nanofibers

Carbon nanofibers (CNFs) offer improvements similar to CNTs in terms of enhanced tensile strength, flexural strength and crack resilience [15, 16]. CNFs owe crack bridging capability at nano level, and establish strong interfacial bond with cement products [17]. Studies show that CNFs enhance ductility, fracture toughness, modulus of elasticity and also contribute to add in high-density C-S-H gel which gets reflected in higher mechanical strength [17-19]. Carbon nano fibers possess high thermal and electrical conductivities, high stiffness, specific strength, tensile modulus, corrosion and chemical resistance, that render them suitable to be intruded as reinforcement to attain superior cementitious matrices [20-22]. Strength to weight ratio of CNFs is greater than steel [23]. CNFs provide better performance compared to CNTs because of higher aspect ratio, which can arrest the nano-cracks more effectively [24]. Fiber spacing is reduced due to nano scale diameter of CNFs that should theoretically delay the formation and propagation of micro cracks at the very beginning. CNFs have 100 times lower production cost than CNTs yet offers similar improvements in mechanical properties, microstructural refinement and other multifunctional properties of concrete [23]. Sanchez et.al reported that CNFs are thermally stable and have higher heat resistance at elevated temperatures as compared to MWCNTs [26].

Table 1: Properties of carbon nano fibers

Fiber diameter (nm)	20-80
Fiber Length (nm)	5000-50000
Purity %	>97
Fiber density (g/cm^3)	2.1
Fiber specific surface area (m^2/g)	70-140

2.7 Dispersion and characterization of carbon nanofibers (CNFs)

Carbon nanofibers get attracted to each other due to presence of strong van der Waal's forces which leads to formation of agglomerates as they get entangled and closely packed [16]. In order to achieve efficient dispersion, chemical methods (use of surfactant) are applied in conjunction with physical aids (ultrasonication). For the homogenous dispersion of carbon nano-media, surfactant should complement the chemistry of the host matrix [43]. Literature reports the use of

Gum Acacia (GA) which is proved to be beneficial to disperse carbon nanomedia and compliments the fresh mix and hardened properties of cement matrix [44, 45]. In this study, surfactant-ultrasonication technique is employed in conjecture with a natural surfactant (Gum Acacia) to weaken the surficial attractive forces. To attain homogeneous suspension of CNFs in mixing water, aqueous dispersion by adding weighed carbon nanofibers to GA solution were made before applying sonication. CNFs-surfactant ratios are chosen in the range of 1:0 to 1:6. To ensure higher level of dispersion and de-agglomeration for the resulting suspension, sonication was performed with a cup horn ultrasonicator at a controlled amplitude of 70%. The dispersion of CNFs was assessed by measuring the absorbance spectra using UV-visible spectroscopy. For each suspension absorbance at 500 nm wavelengths were measured as it remains unaffected at ambient settings [45]. When sonication energy was applied for 45 minutes, it is observed that the CNFs-surfactant ratio of 1:1 resulted in optimal homogenous and stable suspension as shown in Figure 6.
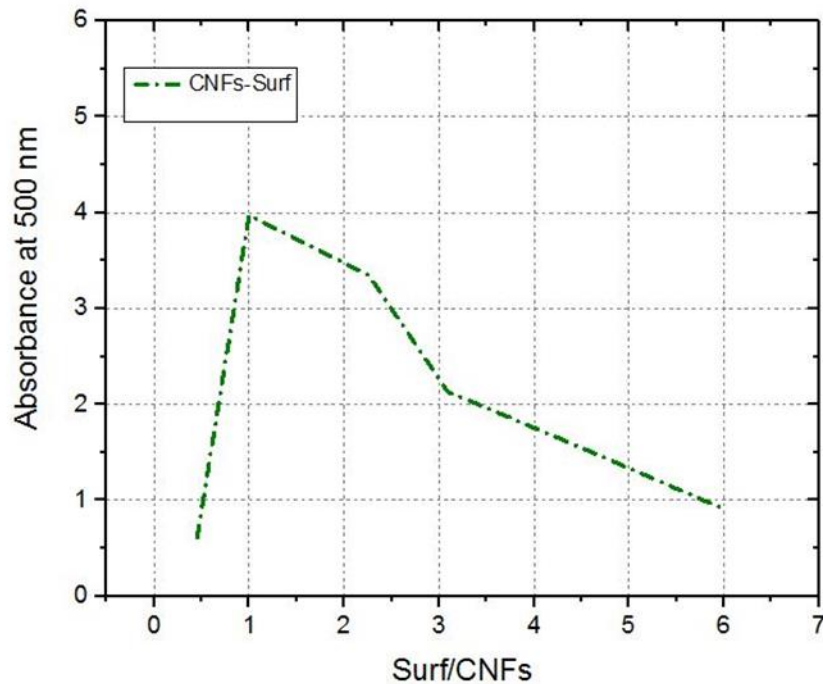
Figure 6: UV-Vis Spectroscopy of Gum Acacia with Carbon nano fibers

2.8   Basalt Fiber (BF)

Basalt fibers (BF) is a inorganic fiber that is extruded from melted basalt rock in temperature between 1460°C to 1500°C [27]. BF recently gained popularity in structural applications owing to its substantial strength and modulus, high resistance against chemical attack and extended operating temperature range (−200°C to 600°C). Similarly, its fire resistant properties [28, 29], environmental friendliness, higher impact load capacity, and commercial availability are among the factors for its widespread use [30]. Chopped Basalt fiber is shown in Figure 7.

Figure 7: Chopped basalt fiber

2.9   Properties of Basalt fiber

Currently, numerous organic and inorganic fibers are available in construction market, however many of them either lack durability or structural strength or are extremely costly for use in moderate loadings. In present times, basalt fiber (BF) is the demanding fiber that is being used in construction industry. Because of novelty of basalt fiber it is extruded from inorganic basalt rock in temperature between 1460 °C to 1500 °C [27] and have recently gained popularity in structural applications owing to its considerable mechanical strength, high modulus, high chemical resistance, thermal stability, extended operating temperature range (−200 °C to 600 °C), non-

combustible characteristics [28, 29] environmental friendliness, higher impact load capacity, and fire with less poisonous fumes and commercial availability [30].

Tensile strength of BF is higher compared to E-glass fiber, BF has higher strain at failure compared to carbon fiber (CF). In addition to that it has excellent resistance against impact load, chemical attack and creates less poisonous fumes in fire [31]. Adding economical cost of BF to its properties, this makes basalt fiber an appropriate alternative for steel, glass and carbon fibers in many construction works [32, 33]. For building structures, when adequate structural properties and enhanced fire resistance are all together required, cementitious composites reinforced with BF can be a better replacement to conventional matrices reinforced with fiber as when tested under 600°C merely BF maintained its 90% of strength plus volumetric integrity than glass and carbon fibers [33]. The manufacturing process of BF is analogous to that of glass fiber, but with less energy consumed and no additives, that makes it inexpensive compared to GF and CF [34-36]. Additional benefits such as higher heat resistance, modulus, better endurance against chemical attack, exceptional interfacial shear strength and commercial availability, enable basalt fiber a good replacement to GF or CF [37]. Tehmina Ayub et.al found with BFs intrusion, tensile strength and the flexural strength of the HPFRC significantly improved [46]. Such improvements in tensile and flexure capacity are sought after in fire resistance studies. Diameter of basalt fiber is larger than 9 microns and they are safe for health so they are not inhalable materials. Because of this property, basalt fibers have been recently categorized as "The green industrial material for the twenty-first century" [47].

Table 2: Manufacturer provided properties of BFs

Fiber diameter (um)	16-18
Fiber Length (mm)	12.7
Density (g/cm^3)	2.67
Tensile Strength (MPa)	3500
Elastic Modulus (GPa)	80

2.10 High Strength Concrete (HSC)

High strength concrete is a type of high-performance concrete (HPC), usually having a compressive strength of 40 MPa or more. For the production of high strength concrete (HSC); quality control and greater research is required as compared to conventional concrete [48]. In today's world, concrete with high strength is used and for its production, the ratio of water to binder are reduced and super plasticizers are used in the concrete for that purpose. Also, to achieve low porosity and permeability, different types of cement replacement materials can also be added to concrete. Silica fume can be added in concrete which results in decrease in porosity, permeability and bleeding. It is one of the most popular pozzolans because their oxides (SiO_2) react and utilize calcium hydroxides that are hydration products of ordinary Portland cement. Lower release of heat, development of greater strength, consumption of lime and smaller pore size distribution are the major results of pozzolanic reactions [49].

2.11 Silica Fume

Ferrosilicon and silicon industry produce silica fume (SF) as a byproduct. At 2000°C, SiO2 vapors are formed by reduction of quartz to silicon. These vapors in the zone of low temperature oxidize and condense to form little non-crystalline silica particles. The percentage of SiO2 in silica depends upon the alloy used [50]. Normally it is found in grey or premium white color [51]. SF particles are very fine, spherical and amorphous contains small amounts of alkali oxides. SF is commonly utilized for making high strength concrete. Below are the important advantages of SF.
• By using SF, we can get higher early compressive strength
• Higher modulus, tensile and flexural strength
• By using SF, toughness and bond strength can be increased
• Durability is enhanced
• Abrasion resistance is increased

2.12 Reaction mechanism of silica fume

SF has finer amorphous silicon dioxide particles that make SF a very reactive pozzolanic material. Basically, SF has three major roles in concrete: (i) Provide dense matrix and reduce the pore size (ii) SF reacts with free lime and produce CSH gel and (iii) refinement of cement paste-aggregate

interfacial. SF particles size is very small and they provide the site for nucleation and also react with free lime to form gel. It also changes the orientation of CH crystals and also reduces the transition phase. Hence, improved mechanical properties and enhanced durability can be achieved by using SF [51].

2.13 Testing method based on loading and heating regime

Most of the test programs aimed at studying the deterioration of the material properties of concrete under elevated temperatures mostly use three type of test methods namely stressed, unstressed and unstressed residual property tests. In the stressed test condition load of magnitude which is 40% of member capacity is applied in pre-heating stage of test. The member is heated at a given heating rate up to the desired temperature after which the temperature is kept constant and is prevented to further increase in temperature. The remaining load is then applied with the desirable rate as shown in Figure 7 To perform test under this loading and heating regime, a sophisticated assembly of furnace and loading machine is needed i.e. sample is placed in the furnace while load is being applied on it. It is a complex system and not available commonly in structure engineering laboratories as special arrangements are required. The laboratories specially established to study the fire properties of structures mostly are equipped with this facility. This loading and heating regime truly depict the actual scenario of structures under fire event. The second testing scenario is unstressed test conditions. Under this condition, the specimen or member is not loaded in preheating conditions. In contrast to stressed method, the member or specimen is kept free from any loading and heating is applied at desired target rate till the given temperature. This temperature is then kept constant and load is applied at a desired rate up to the failure of the structure. This heating and loading regime does not truly depict the actual structural conditions under fire. This testing condition finds its importance due to unavailability of stressed test condition equipment. The results obtained from unstressed test conditions although different from stressed conditions in magnitude but they follow the same trend and the structure under fire behave
in a similar fashion in both these testing conditions. This testing and heating regime is shown in Figure 8. In residual test conditions the concrete specimen is exposed to target temperature at a

desired rate and then allowed slowly cool down. When the temperature of the member or specimen
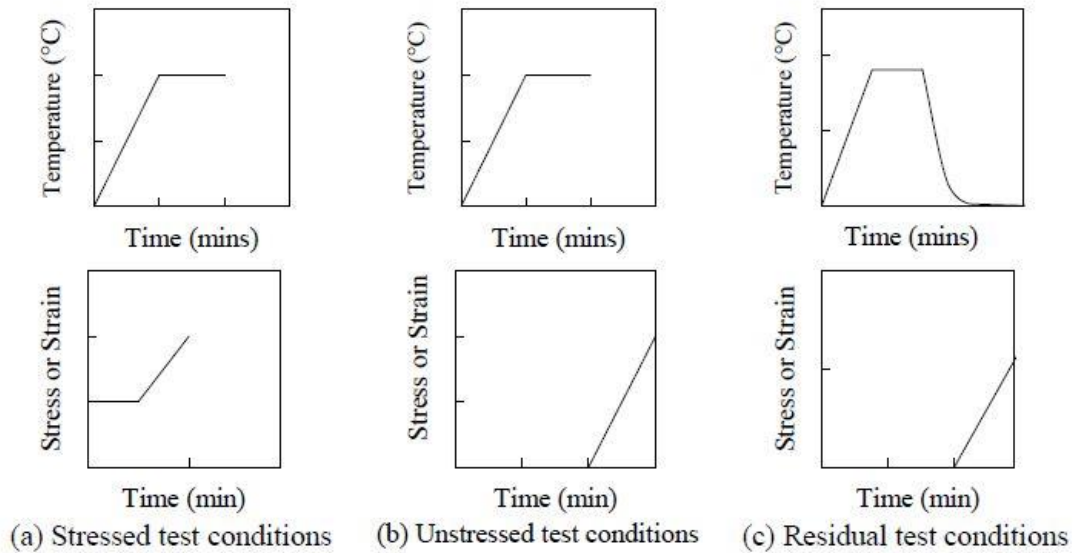
Figure 8: Heating and loading regimes for different test conditions

is in equilibrium with ambient conditions, then member or specimen is loaded up to failure.

2.14 Previous investigations on mechanical performance of concrete exposed to elevated temperatures

This section presents a brief review of the published data on the variation of compressive strength, splitting tensile strength, elastic modulus, compressive stress-strain behavior and mass loss at different elevated temperatures. The variation of these aspects of concrete are sensitive to many factors i.e. heating rate, test methods (stressed, unstressed or unstressed residual), size of the test specimen, moisture content during heating, type of coarse aggregates, strength (NSC or HSC), cement content, type of SRM (fly ash, silica fume etc.), type of cement and so on. Considering each individual factor from each study for comparison purposes is not possible because all of the information is seldom found in a particular study. A general review of the studies on fire behavior of concrete is presented.

2.14.1 Compressive strength

Compressive strength is the most fundamental and important mechanical property of concrete as it is the basic input parameter in the structural design of RCC elements. In majority of the grey structures, concrete is structurally active in compression. For the development of the predictive models of the structural performance of RCC elements exposed to elevated temperatures, the variation of the compressive strength of concrete as a function of temperature must be known as an input parameter. Lawson et.al presented [52] a review of a number of studies on the variation of compressive strength of concrete with increasing temperatures and concludes that the variation of compressive strength of concrete as a function of fire is subjective to a number of parameter i.e. strength at room temperature (NSC or HSC), nature of loading and heating regimen (stressed, unstressed or unstressed residual), heating rate, type of coarse aggregate (normal weight siliceous and calcareous, or lightweight), moisture content and the porosity of concrete which is highly affected by the presence of SRM (SF, FA and GGBFS etc.).

Degradation of compressive strength as a function of temperatures is more pronounced in the case of HSC in comparison to NSC owing to the fact that microstructure of HSC is denser and impermeable, so the steam pressures generated due to the high temperatures don't get escaped. In terms of relative compressive strength loss, HSC losses up to 40% of its room temperature strength between the temperature range of 100°C to 400°C where as in same temperature range, NSC losses 10 to 20 % of its room temperature strength [52]. SRMs have been recognized to be essential ingredients for producing high performance concrete (HPC). SRMs not only make the concrete production economical but also their optimum use can result in a superior concrete as compared to conventional concrete. Presence of a particular SRM in concrete may effect fire behavior of concrete either adversely or beneficially. Presence of FA and GGBFS has been reported to improve the response of concrete under fire while presence of SF and MK has been reported to adversely affect the response of concrete under fire [53]. Table 3 gives the details about the test programs carried by different researchers to evaluate the performance of mixes containing SRMs.

Table 3: Details of test programs pertaining to fire behavior of different mixes containing various SRMs.

SRM	Author	Short Name	w/c ratio	OPC (Kg/m^3)	SRM (Kg/m^3)	Heating Rate	Testing Method
Fly ash Concrete	(Xu et al. 2001)	FAC	0.30	225	275	1°C/min	unstressed residual
Silica fume Concrete	(Behnood and Ziari 2008)	SFC	0.30	450	45	3°C/min	unstressed residual
Metakaolin Concrete	(Poon et al. 2003)	MKC	0.30	400	100	2.5°C/ min	unstressed residual
Blast Furnace slag Concrete	(Siddique and Kaur 2012)	SC1	0.45	180	270	8°C/min	unstressed residual
Blast Furnace slag concrete	(Xiao et al. 2006)	SC2	0.34	261	261	25°C/ min	unstressed residual

Recent study [54] evaluated the the effects of two different cement contents i.e. 250 and 350 kg/m^3 on the behavior of concrete under elevated temperatures. He used limestone aggregates, ordinary Portland cement (OPC), a fixed w/c ratio of 0.50 and a heating rate of 2°C/min. Test specimens used for compressive strength tests were cubes having dimensions 150X150X150 mm. The room temperature compressive strengths were 28.16 and 48.99 MPa of mixes having cement contents of 250 and 350 kg/m^3 respectively. He studied the variations in compressive strength under unstressed residual conditions after the exposure of test specimens to five different target temperatures i.e. 100, 200, 400, 600 and 800°C. Each temperature was maintained for 45 minutes so that each specimen could attain thermal steady state. He made conclusion that cement dosage didn't affect the behavior of concrete under elevated temperatures to a greater extent.

The compressive strength of concrete exposed to elevated temperature is a considerable attention in fire resistant design. According to Yuzer [55], strength loss can be due to the thermal incompatibility between the cement paste and the aggregates. Additives can enhance the properties of concrete subjected to high temperatures [56]. Rate of heating and heating temperature also affect concrete properties subjected to elevated temperature. Higher vapor pressure develops due to rapid

heating rate and results in cracks in concrete. Compressive strength of concrete starts to reduce when concrete heated at 200°C and above that temperature [57]. The decrease in compressive strength of concrete after exposure to elevated temperatures was because of dehydration of hydrates of ettringite, CSH gel and the expulsion of capillary pore water [58, 59]. Considerable decrease in strength has been reported above 800°C. The higher decrement in strength can be because of de-hydroxylation of calcium hydroxide [59]. The micro-cracks formation in the samples caused the decrement in strength because of transitions in the cement aggregates bond and changes in the interfacial transition zone [80]. As reported by Phan.et.al, the explosive spalling of concrete at elevated temperature is because of the internal pore pressure development and thermal stresses which further reduces the strength [60].

Sofren and Takashi [61]in their study concluded that residual compressive strength of high strength concrete at high temperature reduces to 20% and 36% at 200°C and 400°C respectively as compared to room temperature. Khaliq and Waheed [62] in their work on high strength concrete concluded that unstressed compressive strength of high strength concrete samples were 67%, 67.5%, 53% and 37% at 100, 200, 400 and 600°C respectively as compared to room temperature. Huzeyfa and Nilufer [63] in their work reported that strength reduces with the increase in temperature and also decreases more in smaller size samples. They also concluded that samples having air entrainment agent and fibers shows greater residual strength as compared to controlled specimens. Khaliq and Taimur [64] in their work on mechanical properties of recycled aggregates HSC at elevated temperatures, compared unstressed and residual test conditions. Results indicate that at 100°C, the loss in compressive strength was 12% for residual test condition and 22% for unstressed test condition. At 800°C, the compressive strength was 7% for unstressed test condition and 5% for residual test condition.

Behnood et.al [56] concluded that silica fume increased the strength because silica fume react with calcium hydroxide and formed calcium silicate hydrate (CSH) gel. Silica fume also act as a filler and reduced the porosity. Reductions in strength occurred in the temperature range of 300-600°C, which were 68.8%, 70.9% and 73.2% in concrete containing 0%, 6% and 10% of silica fume, respectively. At elevated temperature, the cement paste and aggregates bonding weakened due to cement paste contraction and aggregates expansion and consequently significant reduction in strength occur. Phan and Carino [65] in their research worked on three conditions of heating. For

temperatures of 100 and 200^{0}C, the residual property test method showed lowest strength loss. For 450^{0}C, the strength loss was highest for the residual property test condition.

Natinger et.al [66] studied performance of concrete exposed to elevated temperature with the effect of two different kinds of aggregates i.e. dolomite (calcareous) and diabase (siliceous) aggregates. He used OPC, a fixed cement content of 450 kg/m3 and a fixed w/c ratio of 0.50. The room temperature compressive strengths of concretes containing calcareous (dolomite) and siliceous (diabase) aggregates were 45.9 and 38.3 MPa respectively. Specimens used for compressive strength tests were 4X4X8 cm prisms. Concrete specimens were heated for a duration of 1.5 hours in an electric furnace which was preheated to five different target temperatures i.e. 200, 400, 600, 800 and 1000°C. Concrete specimens were cooled down to ambient temperature after exposure to high temperatures, and then were loaded to for strength test. He concluded that in the temperature range of 200°C to 400°C, the deterioration of compressive strength with increasing temperatures is lesser for concrete containing siliceous (diabase) coarse aggregates whereas at temperatures beyond 400°C, the degradation of compressive strength was lesser for concrete containing calcareous (dolomite) aggregates.

2.14.2 Tensile strength

Concrete is very weak in tension and therefore it cracks very early when it is subjected to tensile state of stress. Tensile strength of concrete is about 7 to 11% of its compressive strength and the main reason behind very low tensile strength of concrete is the ease with which cracks can propagate through the structure of concrete under tensile state of stress [67]. This is the reason that the tensile strength of concrete is usually ignored in the structural design of RCC elements. In connection with the fire behavior of concrete, particularly in the case of HSC tensile strength is of key importance due to the occurrence of explosive spalling [68]. Explosive spalling of concrete's specimens is influenced by number of factors including the permeability of concrete, tensile strength of concrete, size of the test specimens and type of fire exposure [7]. There are three methods of determining the tensile strength of concrete namely direct tension test, splitting tensile strength test and third point flexural loading test. Determination of tensile strength through direct tension test is not used commonly as it is unreliable because the specimen holding arrangements can introduce secondary stresses which may become too significant to be ignored [67]. Therefore,

two methods which are commonly used for the determination of tensile strength of concrete are splitting tension test and third point flexural loading test.

Khaliq and Kodur [68]studied the variation of splitting tensile strength of three types of HSC mixes namely self-compacting mix (SCC), fly-ash mix (FAC) and a conventional high strength concrete mix (HSC). Room temperature compressive strengths of SCC, FAC and HSC mixes were 72 MPa, 98 MPa and 90 MPa respectively. Room temperature splitting tensile strengths of SCC, FAC and HSC were 3.9 MPa, 3.3 MPa and 4.6 MPa respectively. They used a heating rate of 2°C/min, a hold time of 2 hours and seven target temperatures i.e. 100, 200, 300, 400, 500, 600 and 800°C. They used unstressed test method for high temperature testing.

Tanyildizi and Coskun [69] studied silica fume behavior at high temperature by using 10%, 20% and 30% silica fume. Results showed that silica fume addition helped to better retain the tensile strength of concrete. Sofren and Takashi [61] in their research work concluded that residual tensile strength reduces to 16% and 30% at 200oC and 400oC, respectively, as compared to room temperature tensile strength.

Khaliq and Waheed [62] in their work on high strength concrete concluded that unstressed splitting tensile strength of high strength concrete samples were 72%, 73%, 55% and 24% at 100, 200, 400 and 600oC, respectively, as compared to room temperature. Khaliq and Taimur [64] in their work compared unstressed and residual test conditions. They concluded that there are no considerable differences in tensile strength response under unstressed and residual test methods. At 800°C, the tensile strength was 16% as compared to room temperature tensile strength.

Behnood et.al [7] investigated the variation of splitting tensile strengths as a function of temperatures for two OPC concrete mixtures and two SF mixtures. OPC mixtures were designated as OPC-30 (w/c ratio of 0.30) and OPC-40 (w/c ratio of 0.40). SF mixtures were designated as SF-6 (6% cement replacement) and SF-10 (10% cement replacement). W/c ratios of SF-6 and SF-10 mixes were 0.35 and 0.30 respectively. Room temperature compressive strengths of OPC-30, OPC-40, SF-6 and SF-10 were 67.8, 61.3, 74 and 84.25 MPa respectively. Room temperature splitting tensile strengths of OPC-30, OPC-40, SF-6 and SF-10 were 5, 4.37, 5.55 and 6.55 MPa respectively. They employed a heating rate of 3°C/min and a hold time of three hours. The target temperatures were 100, 200, 300 and 600°C. The high temperature test method was unstressed-residual.

2.14.3 Compressive stress-strain response

Compressive stress-strain response of concrete is of fundamental importance as it is a necessary input parameter in the mathematical models used for predicting the response of a concrete structural member. For simulating the response of a concrete structural member exposed to fire using a numerical method i.e. finite element analysis, the constitutive model of concrete must be available which could capture the strains at various stress levels at different temperatures. With the increase in temperature, concrete becomes more and more porous, and this increase in porosity causes a more and more ductile behavior of concrete in compression. Therefore, the slope of stress-stain curves decreases with the increase in exposure temperatures [70]. The strains corresponding to peak stresses and ultimate stresses also tend to increase with the increase in elevated temperatures [71].

Diederichs et.al [72] measured the stress-strain response of HSC mixes containing FA under unstressed conditions. The heating rate was 2°C/min and the exposure temperatures were 250, 450, 550, 650, 750 and 850°C. They employed strain-controlled scheme for capturing the stress-strain response. The specimens were 80 X 300 mm cylinders and the room temperature compressive strength was 91.8 MPa. Cheng et.al [73] studied the stress-strain behavior of HSC at different elevated temperatures under residual conditions. Heating rate was 2°C/min. The room temperature compressive strength was 71.4 MPa. The test specimens were 100 X 200 mm cylinders. The employed strain-controlled loading scheme for measuring stress-strain response. They found that the slope of stress-strain plots decreases with an increase in exposure temperatures. They also found that the peak strains at elevated temperatures can be as large as four times the corresponding peak strains at room temperatures.

2.14.4 Elastic modulus

Modulus of elasticity of concrete is a fundamental material property as it is essential input parameter for determining the deflections of a concrete structural element. It is also a compulsory input parameter for carrying out elastic frame analysis of RCC frames. Elastic modulus of concrete mostly depends on w/c ratio, age of concrete, methods of conditioning after casting of concrete, type of aggregates and amount of aggregates [70]. Like other material properties of concrete, its elastic modulus also varies as a function of temperature.

Xiao et.al [74] studied the variation of elastic modulus as a function of temperature. They used a heating rate of 2.5°C/min and a hold time of 2.5 hours. The water to cement ratio was 0.24, powder content was 580 Kg/m^3, 20% mass of cement was replaced with GGBFS and 10% cement mass was replaced with SF. The room temperature compressive strength and elastic modulus of HSC were 68.36 MPa and 38.22 GPa respectively. The specimens were 100 X 100 X 300 mm prisms. They found a severe drop in elastic modulus in the exposure range of 23 to 200°C. This drop became a little steady from 200 to 400°C but the most pronounced rate of degradation was observed from 400 to 600°C. At temperatures beyond 600°C, a drop in rate of reduction of elastic modulus was observed. They attributed the reduced rate of drop in elastic modulus beyond 600°C to the calcination of limestone aggregates.

Khaliq and Waheed [62] concluded that elastic modulus of high strength concrete samples reduces as the temperature is increased and it reduced to 40% at 600°C.

Sofren and Takashi [61] in their research work concluded that elastic modulus of high strength concrete subject to high temperature reduces to 25% and 57% at 200°C and 400°C, respectively, as compared to room temperature.

Khaliq and Taimur [64] in their work compared unstressed and residual test conditions. They concluded that loss in elastic modulus was more under unstressed test condition as compared to residual test condition. They also concluded that in unstressed test condition, the loss in elastic modulus was 26%, 67.7% and 87.3% at 400, 600 and 800°C, respectively, as compared to room temperature.

2.15 Effect of CNFs and BFs on Cementitious composites and Concrete

Concrete being a quasi-brittle composite, when exposed to fire conditions is vulnerable to deterioration because of initiation and promulgation of the induced cracks [75]. The phenomenon of cracking initiates at nano scale, these cracks then assimilate into micro cracks and ultimately develop as macro cracks. Due to accumulative action of vapor pressure and thermal non-uniformity as explained in preceding section, a roll on effect is often observed resulting in badly cracked concrete matrices. Concrete being weak in tension and of brittle nature is inept to restrain these cracks [43, 45]. Several techniques have been used to coup the cracking behavior of high strength concrete at elevated temperatures, among these techniques, the incorporation of fibers into concrete to attain direct mechanical enhancement by delaying transformation of micro-cracks into macro-cracks has been established as the most effective approach [76]. To enhance ductility,

tensile capacity and thermal endurance of HSC, intrusion of synthetic and natural fibers such as steel [77], polypropylene [78] and glass fibers [79] have been sought. Inclusion of steel fibers improves crack resistance, ductility and tensile strength of HSC, thus helps mitigate spalling by crack bridging and uniform scattering of thermal stresses [76]. However, the use of steel fiber increases the unit load of concrete which results in thicker foundations and is deemed uneconomical. Further, durability related issues arise in cold areas where freeze-thaw and de-icing is common which corrodes the steel fibers, thus weakens the interfacial bond and induces expansive cracks. It has been observed that due to excessive corrosion concrete cover spalls off giving way to other deleterious agents [80]. These reasons hinder the widespread use of steel fibers in fire resistant concrete. Similarly, spalling in HSC can also be mitigated with the addition of polypropylene fibers (PP). These fibers typically melt at low temperatures between 170-250℃ to create channels to instigate the dissipation of pore pressure buildup in the concrete by forming micro-macro pores (openings) [76]. However, the presence of macro-pores in PP reinforced concrete adversely affect the post fire durability of such concretes [81].

Cracking in the concrete initiates at nanoscale level and traditional fiber reinforcement is not effective to curtail it. In recent times the use of nano-materials has unveiled a novel mechanism to hinder the formation and propagation of nanoscale cracks by crack bridging and improved mechanical performance with densification of interfacial transition zone [82, 83]. Waqas et.al [45] studied the impact of CNTs on concretes exposed to elevated temperatures and found that, CNTs act as nano reinforcements that bridge the cracks produced as a result of pore pressure accumulation. Also the highly thermally conductive nature of CNTs was deemed useful. CNTs helped reduce the thermal inertia by acting as a conductor of heat in the incumbent matrix. Similarly, it was found that the CNTs can also help scatter the thermal stresses. Zechuan et.al [84] reported that the introduction of CNTs as a thermally stable reinforcement can significantly enhance tensile strength of concrete both at ambience and elevated temperatures. Bastami et.al [85] demonstrated that nano silica, if efficiently used in HSC can improve its mechanical properties at elevated temperatures. The results show that the presence of nano silica increased residual compressive and tensile strengths, curtailed spalling and reduced the total mass loss.

Carbon nanofibers (CNFs) offer improvements similar to CNTs in terms of enhanced tensile strength, flexural strength and crack resilience [15, 16]. CNFs owe crack bridging capability at

nano level, and establish strong interfacial bond with cement products [17]. Studies show that CNFs enhance ductility, fracture toughness, modulus of elasticity and also contribute to add in high-density C-S-H gel which gets reflected in higher mechanical strength [17-19]. Carbon nano fibers possess high thermal and electrical conductivities, high stiffness, specific strength, tensile modulus, corrosion and chemical resistance, that render them suitable to be intruded as reinforcement to attain superior cementitious matrices [20-22]. Strength to weight ratio of CNFs is greater than steel [23]. CNFs provide better performance compared to CNTs because of higher aspect ratio, which can arrest the nano-cracks more effectively [24]. Fiber spacing is reduced due to nano scale diameter of CNFs that should theoretically delay the formation and propagation of micro cracks at the very beginning. CNFs have 100 times lower production cost than CNTs yet offers similar improvements in mechanical properties, microstructural refinement and other multifunctional properties of concrete [23]. In addition to that, physical configuration of CNFs offers numerous exposed edges along the surface, which in turn concocts potential sites of interfaces for hydration products to grow [86]. Sanchez et.al reported that CNFs are thermally stable and have higher heat resistance at elevated temperatures as compared to MWCNTs [26]. The aforementioned properties inspired us to evaluate the fire endurance of concrete with the integration of CNFs.

Currently, numerous organic and inorganic fibers are available in construction market, however many of them either lack durability or structural strength or are extremely costly. In present times, BF is the demanding fiber that is being used in construction industry. Because of novelty of basalt fiber it is extruded from inorganic basalt rock in temperature between 1460 °C to 1500 °C [27] and have recently gained popularity in structural applications owing to its substantial mechanical strength, high modulus and chemical resistance, thermal stability, extended operating temperature range (−200 °C to 600 °C), non-combustible characteristics [28, 29] environmental friendliness, higher impact load capacity, and fire with less poisonous fumes and commercial availability [30]. Tensile strength of BF is higher compared to E-glass fiber, BF has higher strain at failure compared to carbon fiber (CF). In addition to that it has excellent resistance against impact load, chemical attack and creates less poisonous fumes in fire [31]. Adding economical cost of BF to its properties, this makes basalt fiber an appropriate alternative for carbon, glass and steel in many construction

works [32, 33]. For building structures, when adequate structural properties and enhanced fire resistance are all together required, cementitious composites reinforced with BF can be a better replacement to conventional matrices reinforced with fiber as when tested under 600°C merely BF maintained its 90% of strength plus volumetric integrity than glass and carbon fibers [33]. The industrial development of BF is comparable to that of glass fiber, but with less energy consumed with no additives, that makes it inexpensive compared to GF and CF [34-36]. Additional benefits such as higher heat resistance, modulus, better endurance against chemicals, exceptional shear strength and market availability, enable basalt fiber a good replacement to GF or CF [37]. Tehmina Ayub et.al found with BFs intrusion increased the flexural and tensile strength of high performance fiber reinforced concrete [46]. Such improvements in tensile and flexure capacity are sought after in fire resistance studies. Diameter of basalt fiber is larger than 9 microns and they are safe for health so they are not inhalable materials. Because of this property, BFs have been categorized as "The green industrial material for the twenty-first century" [47].

CHAPTER 3

EXPERIMENTAL PROGRAM

3.1 General

Studying the behavior of HSC reinforced with carbon nano fibers and basalt fibers subjected to elevated temperature needs a detailed test program with various concrete mix regimes. The test program must include basic mechanical testing of concrete specimens including compressive and split tensile strength tests, stress strain plots, elastic modulus, compressive toughness, and mass loss. High strength concrete is discussed in details in the literature by various authors but there is no single series of tests available which covers the mechanical properties of CNFs and BFs intruded high strength concrete under fire. In order to understand the fire and spalling behavior of high strength concrete, basic mechanical tests namely compressive and splitting tensile strength test, stress strain response, elastic modulus, and mass loss are performed at temperatures of 23, 100, 200, 400, 600 and 800°C under residual test conditions. The details about test program and procedure, materials and mix regime are discussed in details in this chapter. All the mechanical and material properties thus evaluated are presented in form of graphs, and generated data was compared with control mixes as well. The collected data was utilized to develop simplified mathematical models for various material properties of these modified mixes as a function of temperature in range of 23-800℃. This chapter presents the details about the materials, methods and procedures used in this study.

3.2 Design of material property experiments

Test program was carried out elevated temperature material property tests on all five formulations of concretes. Cylindrical specimens of dimension (200mm height x 100mm diameter) were fabricated from each bath of concrete mixes. After curing the specimens for 28 days, these specimen were exposed to different temperatures ranging from 23-800℃ to evaluate the high temperature material properties for all formulations. Due to lack of standardized test methods for the high temperature strength tests on concrete in ASTM standards, RILEM [87, 88] guidelines were adopted to high temperature material and mechanical properties of HSC, 0.1CNF-HSC, 0.2CNF-HSC, 1B-HSC and 2B-HSC respectively. Special handling techniques were employed for transfer of samples from furnace to strength testing machine, for compressive strength tests and

stress-strain tests. A specially designed steel bracket was used to carry out splitting tensile tests at elevated temperatures. Residual test method was used to study the elevated temperature mechanical and material properties of the mixes. The material properties of all types of concretes (HSC, 0.1CNF-HSC, 0.2CNF-HSC, 1B-HSC and 2B-HSC) were evaluated using this test method.

3.3 Materials

In this section materials used in experimental study have been discussed. Ordinary Portland cement (OPC) Type-I in compliance with ASTM C150 [89] is utilized as a primary binder for the analyzed formulations. River sand is used as fine aggregate having a fineness modulus of 2.7 and limestone coarse aggregate with maximum size of 12.5 mm is used in saturated surface dry (SSD) condition. Physical properties of ordinary Portland cement, fine and coarse aggregates are summarized in Table 4 and Table 5 respectively. Vapor grown CNFs are used as-received from Grupo Antolin Ingenieria, Spain. To effectively disperse nano media in the cementitious matrix, powder of Gum Acacia (GA) was used as a surfactant. Properties of CNFs and Gum Acacia are given in Table 6. Basalt fiber (BFs) are used as-received from Techno-basalt Ukraine. Properties of basalt fibers are given in Table 3. A BF dose of 1 and 2 wt% of cement is added to modified concrete specimens and in parallel to that control samples are prepared for comparison [90]. Ordinary tap water was utilized to for curing of concrete specimens. Type-A plasticizing admixture meeting the requirements of ASTM C494 was used.

Table 4: Ordinary Portland Cement (physical and chemical properties)

Physical Property	Content	Chemical composition	Content %
Insoluble residue (% mass)	0.49	CaO	65.81
Specific gravity (g/cm^3)	3.15	SiO$_2$	18.83
Specific surface area (cm^2/g)	8300	Al$_2$O$_3$	6.94
Particle size (d$_{50}$) (cm)	1.658	Fe$_2$O$_3$	3.47
Loss on ignition (% mass)	2.21	MgO	1.94
		SO$_3$	1.32
		Na$_2$O+K$_2$O	1.2

Table 5: Physical properties of aggregates

Aggregate type	Limestone aggregate	Fine aggregate
Size (mm)	12.5	-
Specific gravity (g/cm^3)	2.48	2.64
Water absorption (%)	2.66	1.62
Bulk density (kg/m^3)	1558	1546
Crushing value	23	-
Fineness modulus	2.8	2.23
Maximum size of aggregate (mm)	12.5	-

Table 6: Properties of CNFs and Gum Acacia

CNFs		Gum Acacia	
Fiber diameter (nm)	20-80	Average particle size (d_{50}) (mm)	207
Fiber Length (nm)	5000-50000	CaO %	49.20
Purity %	>97	Fe_2O_3 %	21.3
Density (g/cm^3)	2.1	SiO %	16.21
Specific Surface Area (m^2/g)	70-140		

3.4   Mix proportion

One control formulation i.e. high strength concrete (HSC) along with four modified high strength concrete formulations containing CNFs and BFs (0.1C-HSC, 0.2C-HSC, 1B-HSC, 2B-HSC) were prepared. A CNF dose of 0.1 and 0.2 wt% of cement is added to modified concrete specimens and in parallel to that control samples are prepared for comparison [19, 91]. A BF dose of 1 and 2 wt% of cement is added to modified concrete specimens and in parallel to that control samples are prepared for comparison [90]. The details of mix proportion for all studied formulations are mentioned in Table 7. Cylindrical specimens of 200 mm height and 100 mm diameter were prepared for high temperature testing. Initial water content is a key factor associated to permeability and density of microstructure in HSC. A low w/c ratio of 0.30 is adopted for all mixes with plasticizer content increasing from 1 to 1.2% wt. Specimen were de-molded after 24 hours and water cured at 23ºC for 28 days. Compressive strength test was performed according to ASTM C39 to evaluate the strength progression of formulations [92]. The incorporation of carbon nano-fibers has improved the compressive strength of 0.1CNF-HSC and 0.2CNF-HSC by 9.8% and 17.6% respectively which is attributed towards the refinement of the microstructure. The addition

of BFs has improved the 28 days compressive strength of 1B-HSC and 2B-HSC by 2.6% and 4.3% respectively. The variation in average cylindrical strengths of modified formulations (1B-HSC & 2B-HSC) containing basalt fibers was found to be in the range of ±4% compared to compressive strengths of control formulation.

Table 7: Mix proportions and compressive strength progression of concretes

Components	Concrete types				
	HSC (Control)	0.1CNF-HSC	0.2CNF-HSC	1B-HSC	2B-HSC
Ordinary Portland cement (kg/m^3)	638	638	638	638	638
Silica fume (kg/m^3)	63.8	63.8	63.8	63.8	63.8
Coarse aggregate (kg/m^3)	1026	1026	1026	1026	1026
Fine aggregate (kg/m^3)	866	866	866	866	866
CNFs (kg) (wt % cement)	-	0.1	0.2		
Basalt fiber (kg) (wt % cement				1	2
w/c	0.30	0.30	0.30	0.30	0.30
28 days compressive strength (Mpa)	49.5	54.39	58.22	50.8	51.6

3.5   Dispersion and characterization of carbon nanofibers (CNFs)

A CNF dose of 0.1 and 0.2 wt% of cement is added to modified concrete specimens and in parallel to that control samples are prepared for comparison [19, 91]. Carbon nanofibers get attracted to each other due to presence of strong van der Waal's forces which results in the creation of agglomerates as they get entangled and closely packed [16]. Chemical methods (such as functionalization, use of a surfactant) cannot overcome van der Waal's forces alone. In order to achieve efficient dispersion and improved dispersion stability, chemical methods are applied in conjunction with physical methods (ultrasonication). For the homogenous dispersion of carbon nano-media, surfactant should complement the chemistry of the host matrix [43]. Literature reports the use of Gum Acacia (GA) which has proved to be beneficial to disperse carbon nanomedia and compliments the fresh mix and hardened properties of cement matrix [44, 45]. In this study, surfactant-ultrasonication technique is employed in conjecture with a natural surfactant (Gum Acacia) to weaken the surficial attractive forces. To assist in the creation of effective dispersion of CNFs in mixing water, aqueous dispersion by adding weighed carbon nanofibers to GA solution were made before applying sonication. CNFs-surfactant ratios are chosen in the range of 1:0 to 1:6. To ensure greater level of dispersion and de-agglomeration for the resulting dispersion, sonication was performed with a cup horn ultrasonicator. To circumvent the hurdle of overheating which is resulted due to sonication energy, aqueous solution is sonnicated at an amplitude of 70%. To validate the dispersion of CNFs, absorbance was performed through a spectrum of wavelengths using UV-visible spectroscopy. For every regime absorbance at 500 nm wavelengths were measured as it remains unaffected at ambient settings [45]. When sonication energy was applied for 45 minutes, it is observed that the CNFs-surfactant ratio of 1:1 produced a highly dispersed solution Figure 9**.**
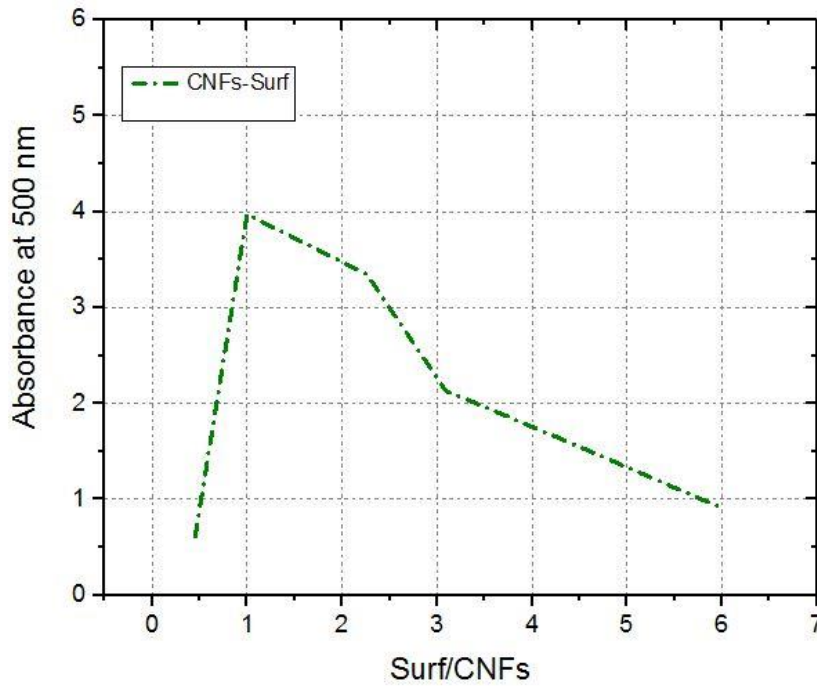
Figure 9: Surf/CNFs vs. Absorbance of CNFs

3.6 Sample preparation

Concrete samples having dimension of 200mm height and 100 mm diameter were cast for each type of formulation. Top surface of freshly prepared concrete was finished by trowel. After pouring, concrete remained in molds for 24 hours then specimens were de-molded and placed in curing tanks with controlled environment of 23℃ temperature and 95% humidity for 28 days. The strength progression was checked by conducting compressive strength tests according to ASTM C39 [92]. Compressive strength tests were conducted on all four concrete types at 7, 14 and 28 days. Results of which are mentioned in Table 8. Splitting tensile strength tests were also done at 28 days for all mixes to get their respective tensile strength.

Table 8: Detail on number of test specimens, temperature levels and test conditions

Mix type	Exposure temperature (°C)	No of samples	Remarks
Cylinder specimen size 100×200 mm and heating rate of 5°C/minute were used.			

HSC	23	6	For residual test conditions
	100	4	
	200	4	
	400	4	
	600	4	
	800	4	
0.1C-HSC	23	6	For residual test conditions
	100	4	
	200	4	
	400	4	
	600	4	
	800	4	
0.2C-HSC	23	6	For residual test conditions
	100	4	
	200	4	
	400	4	
	600	4	
	800	4	
1B-HSC	23	6	For residual test conditions
	100	4	
	200	4	
	400	4	
	600	4	
	800	4	
2B-HSC	23	6	For residual test conditions
	100	4	
	200	4	
	400	4	
	600	4	
	800	4	

For residual test conditions a total of 150 cylindrical specimens of 200 mm height and 100 mm diameter were prepared for high temperature testing, 30 for each batch of formulation. Two concrete specimens were designated at each target temperature for elevated temperature material property tests. For room temperature compressive and tensile strength tests three specimens were tested each. The compression tests and stress-strain tests were coupled together to achieve compressive strength alongside stress-strain curves and eventually elastic modulus. Mass loss calculations were done on samples used for mechanical testing under residual test conditions. Each

data point is an average of two tests, additional tests were performed only if the results were found be extreme outliers. All visual observations were done on residual property test specimens. For microscopic analysis samples were extracted from heat treated and fractured residual test specimens.

3.7   Material property tests

The tests for the determination of mechanical properties tests were performed on heat treated samples under residual condition, material property tests mentioned earlier like compressive and tensile strength, stress-strain response, elastic modulus and mass loss were evaluated. And the details of testing procedure and technique, testing equipment, testing variables and fire loading characteristics are briefly discussed in this section.

3.8   Fire loading characteristics

Test results of the samples exposed to elevated temperatures depend on two basic fire loading characteristics. These characteristics are heating rate and target temperatures. Due to the deficiency of elevated temperature testing standards available, these two characteristics were selected in accordance with prior studies conducted on concrete specimens at high temperatures.

3.9   Target temperature, heating rate and hold time for test method

For elevated temperature properties evaluation of concrete samples, the most frequently used target temperatures are 23℃, 200℃, 400℃ and 600℃. Types of aggregates play a vital role in defining the fire response of concrete as calcareous aggregates tend to desiccate at 800℃. This temperature i.e. 800℃ is also selected for study of microstructure and crack pattern analysis. To evaluate high temperature mechanical properties of concrete the heating rate used by the several researchers lies in range of (2-5℃)/minute. Heating rate varies in case of a realistic fire, sometimes the elevation rate may rise up to 25℃/min [93]. Setting up variable ramp times could turn out to be a difficult task. In the present research a heating rate of 5℃/minute was carefully chosen. The target temperatures achieved in this study are 23°C, 100°C, 200°C, 400°C, 600°C and 800°C. To attain thermal steady state a suitable hold time must be provided to sample under heat treatment. Thermocouple combination of wires which is used to measure temperature, the thermocouples used in present study were type-K. Two thermocouples, one on the surface of the cylinder and one in the furnace were employed to measure the rise of temperature in furnace chamber and on the

surface of cylinder. A suitable hold time of 2 hours and 30 minutes was given for all the mixes, such that they can achieve thermal steady state.

3.10 Test Apparatus and procedure

To attain the compressive and tensile strength, specimens were loaded as per ASTM C39 and ASTM C496 [92, 94] using a load-controlled strength test machine having a capacity of 5000kN connected with a linear variable displacement transducers (LVDTs) and a load cell. A controlled loading rate of 0.2 Mega Pascal per second is applied to sketch the stress-strain curves. Further, these stress-strain response curves were used to compute modulus of elasticity as per the guidelines set in ASTM C469 [95]. Concrete cylinders were exposed to target temperatures by means of an electric furnace to simulate temperatures with a heating capacity up to 1300°C. Furnace was equipped with a digital temperature-time controller to regulate hold times and the heating ramp. To capture temperature variation and to ensure even heat distribution in concrete specimens, two type-K thermocouples were used, one was embedded in the core while other on the surface of representative sample. Temperature measurements for representative samples were taken throughout the tests which helped to validate appropriate hold time and heating rate as per RILEM test procedures [87, 88]. The samples were exposed to target temperatures at a controlled heating rate of 5°C/min. To ensure thermal equilibrium (steady state) conditions a hold time of 2.5 hours (150 minutes) was provided as observed by the time-temperature curves of least thermally conductive matrix (control HSC). Temperature-time variation of control HSC sample is shown in Figure 10. To avoid thermal shock, samples were allowed cool down to ambient temperature with furnace door opened after the provision of hold time. The target temperatures were 23 (ambient temperature), 100, 200, 400, 600 and 800°C. For mass loss measurements, specimens were weighed before and after fire exposure with a weight balance sensitive to 1000th of a gram. Samples were allowed to cool down slowly to ambient temperature with the door of furnace kept open to avoid thermal shock. Prior to strength tests, ultrasonic pulse velocity (UPV) and mass loss test were performed before and after the heat exposure.
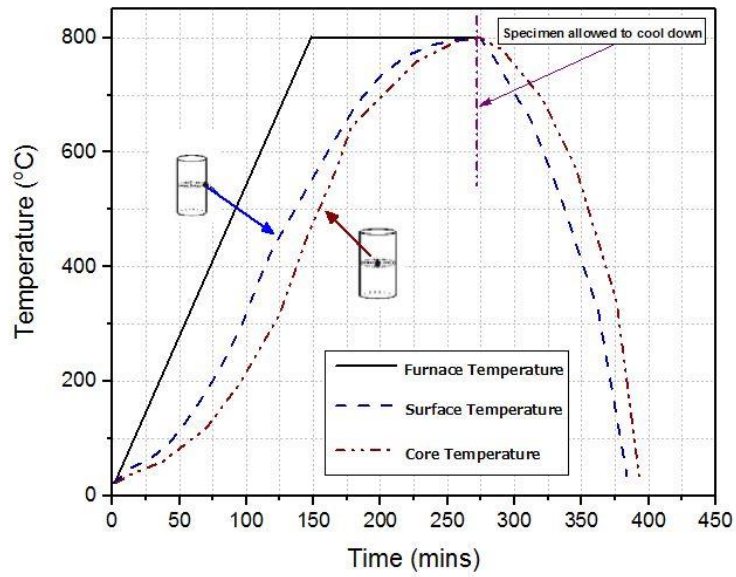
Figure 10: Time-temperature plot depicting furnace and
specimen temperatures for 800ºC heating.

Figure 11: Electric Furnace for heating the samples to targeted temperatures

Figure 12: Strength testing machine

3.10.1 Compressive strength test ($f_{c',T}$)

After achieving the thermal steady state temperature condition, cylinders were allowed to cool down to room temperature in air before they were tested under residual conditions specimens ASTM C39 [93] was followed to determine compressive strength as no testing standards are available in literature which encompass high-temperature compressive testing. Compressive strength ($f_{c',T}$) as a function of temperature were thus evaluated at target temperatures. The loading rate of 0.2MPa per second in compression. Two cylinders were tested at each target temperature. If results were found ambiguous or outliers, additional testing was done to confirm results. To formulate a comparison between results of different concrete types, relative residual compressive strengths were calculated using following relationship.

$$\text{Relative compressive strength} = \frac{\text{Strength at targeted temperature}}{\text{Ambient temperature strength}}$$

3.10.2 Splitting tensile strength ($f_t{}',_T$)

After exposing the samples to target temperatures, samples were allowed to cool down to room temperatures under residual test conditions. The samples were loaded gradually at the loading rate of 0.02MPa per second and the failure load was recorded, the tensile strength ($f_t{}',_T$) were calculated in accordance with ASTM C496 [94]. This test was repeated to confirm results at selected temperatures, where recorded results were unusual or lied outside the tolerance range. To compare tensile strength of different types of concretes, residual tensile strength was calculated using following relationship.

$$\text{Relative tensile strength} = \frac{\text{Strength at targeted temperature}}{\text{Ambient temperature strength}}$$

3.10.3 Stress-strain curve

To plot stress-strain curves, load-deformation data was recorded using data acquisition system attached to compression testing machine and LVDTs. Data was acquired by failing cylinders under gradually rising loads at precise loading rate of 0.2MPa/second. The load-deformation data was used to evaluate stress-strain response of heat treated samples.

3.10.4 Elastic modulus

Secant elastic modulus (E) concrete specimens was evaluated using the stress-strain curves with a relationship described in ASTM C469 [95].

$$E = \frac{S2 - S1}{\varepsilon - 0.000005}$$

E = Chord modulus of elasticity
S2 = Stress against 40% of ultimate load
S1 = Stress against longitudinal strain of 0.00005
ε = Longitudinal strain against S1=0.00005

3.10.5 Mass loss

To observe the variation in mass of heat treated concrete samples, they were weighed before and after heat treatment. For residual conditions, heat treated samples were allowed to cool down to room temperature before mass loss measurements. Relative mass loss measured at different temperatures was calculated from the following relationship.

$$\text{Mass Loss} = \frac{Mt}{M}$$

Mt= Mass at temperature (T)
M = Mass at ambient temperature

3.10.6 Forensic analysis (SEM)

Study of microstructure of all concrete types was done using field emission scanning electron microscope (MIRA3 TESCAN) as shown in Figure 13. Heat treated specimens were visually inspected and samples from broken specimen were taken according to ASTM C1723 for forensic investigation.

Figure 13: Scanning electron microscope

RESULTS AND DISCUSSIONS

4.1   General

This chapter deals with the interpretation of results obtained from experimental work. Dispersion methodology of CNFs has been discussed. Experimental test results of mechanical properties such as tensile strength, compressive strength, stress-strain response, modulus of elasticity, ultrasonic pulse velocity, forensic analysis for microstructure analysis, visual assessment and mass loss are analyzed for high strength concrete and modified high strength concrete with CNFs and BFs.

4.2   Characterization of the degree of CNFs dispersion

Surfactant-ultrasonication technique is employed in conjecture with a natural surfactant (Gum Acacia) to weaken the surficial attractive forces. To assist in the creation of effective dispersion of CNFs in mixing water, aqueous dispersion by adding weighed carbon nanofibers to GA solution were made before applying sonication. CNFs-surfactant ratios are chosen in the range of 1:0 to 1:6. To ensure greater level of dispersion and de-agglomeration for the resulting dispersion, sonication was performed with a cup horn ultrasonicator. To circumvent the hurdle of overheating which is resulted due to sonication energy, aqueous solution is sonnicated at an amplitude of 70%. To validate the dispersion of CNFs, absorbance was performed through a spectrum of wavelengths using UV-visible spectroscopy. For every regime absorbance at 500 nm wavelengths were measured as it remains unaffected at ambient settings [45]. When sonication energy was applied for 45 minutes, it is observed that the CNFs-surfactant ratio of 1:1 produced a highly dispersed solution as shown in Figure 14.
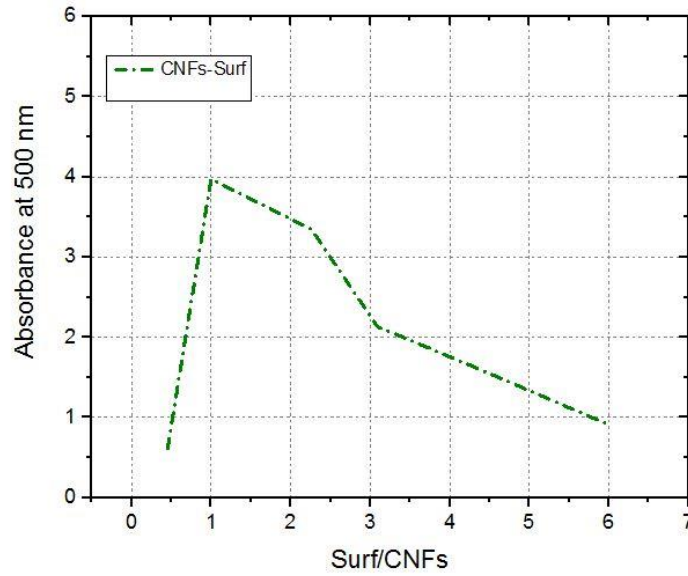
Figure 14: Surf/CNFs vs. Absorbance of CNFs

4.3 Elevated temperature mechanical properties

4.3.1 Compressive strength-CNF-HSC

The ultimate load at which specimens failed at various temperatures was recorded under compression. Relative and absolute residual compressive strength values as a function of temperature are presented in Fig 15.
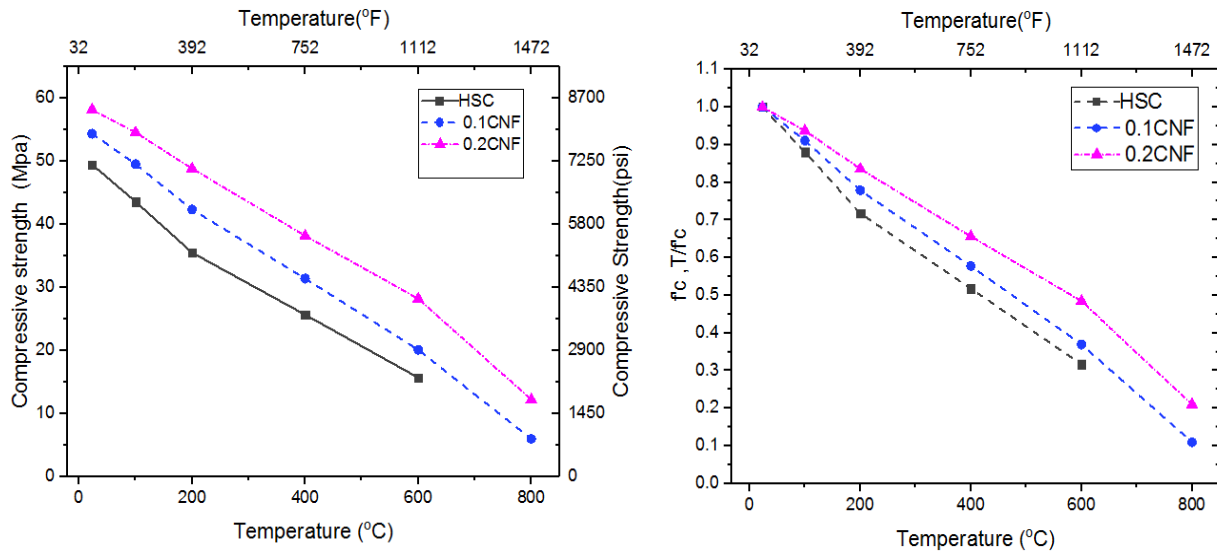
Figure 15: Variation of compressive strength as a function of temperature (a) Absolute

(b) Relative

It can be observed from the trends that both type of concrete i.e. control (HSC) and modified (0.1CNF-HSC & 0.2CNF-HSC) suffer degradation in compressive strength with rise in temperature. This strength loss in compressive strength is unavoidable due to hydrothermal (loss of free and adsorbed water) and numerous physical and chemical changes that occurs in concrete matrix when exposed to high temperatures [96]. First considerable change in hydrothermal condition occurs at 100°C which includes removal of free and adsorbed water, this causes increase in pore pressure that continues to vary up till 200°C [12] causing loss of strength as a result of micro-cracking [97]. A considerable loss of strength occurs at 400°C with the decomposition of calcium silicate hydrate (C-S-H) and calcium hydroxide (CH) which are the main hydrates of cement [7]. The changes above 500°C are not only severe but unalterable [79]. Furthermore, major reason of strength degradation at 600°C is thermal instability of aggregates as de-carbonation of limestone occurs between 600-800°C [12].

The inclusion of nano-fibers refined the microstructure of modified samples (0.1CNF-HSC & 0.2CNF-HSC) which ultimately enhanced the compressive strength initially by 9.8% and 17.6 % respectively at ambient conditions. Nano media were embedded in the host matrix thus improving the microstructure by filling up the voids, and consequently resulted in strength gains. For both

concretes HSC and modified HSC under residual conditions, the relative residual compressive strength loss, follow a similar trend up to 100ºC. However, between 200-800ºC the strength degradation becomes more noticeable in control samples which ultimately spalled above 600ºC. Both the modified formulation performed better in terms of strength retention at all temperatures (23-800ºC) compared to the control HSC. Almost similar behavior of 0.2CNF-HSC compared to 0.1 CNF-HSC up to 100ºC was observed. 0.2CNF-HSC outperformed 0.1CNF-HSC above 400ºC this attributed to the presence of double the amount of thermal conductive media in 0.2CNF-HSC compared to 0.1CNF-HSC. The presence of thermally conductive nanofibers in the cementitious matrices has resulted in uniform distribution of heat, thus mitigating the effects of thermal stresses. The concentration of thermal stresses are the main cause behind the development of heat pockets which result in thermal cracking [45] . This can also be attributed to presence of more nucleation cites in 0.2CNF-HSC as compared to 0.1CNF-HSC. CNFs can provide nucleation sites where the hydrates can grow stably, resulting in high density C-S-H gel [17]. 0.1CNF-HSC and 0.2CNF-HSC retained 40.5% and 51% while control samples retained about 35 % of their strengths at 600ºC. When control HSC spalled above 600ºC, 0.1CNF-HSC and 0.2CNF-HSC still retained 12% and 22% of their strengths at 800ºC. 0.2CNF-HSC has a better relative strength retention of 21% compared to 6% of 0.1CNF-HSC at 800ºC. The presence of thermally conductive media not only helped scatter the thermal stresses effectively but also helped to reduce the thermal inertia [45].

Modified high strength concrete specimens outperformed control samples especially above 400ºC. Microstructural study was performed to analyze the modified samples. Micrograph in Fig 16 shows that CNFs are bridging the cracks hence the presence of CNFs is doubly beneficial i.e. they scatter thermal stress and bridge the cracks which originates as a result of hydrothermal changes. Intrinsic crack bridging nature of CNFs has preserved the effective load-bearing area which in turn has enhances the strength retention. Inclusion of thermally conductive CNFs has increased thermal conductivity (TC) and reduced specific heat in modified specimens. This behavior enables uniform scattering of thermal stresses and reduces the thermal gradient between surface layers and inner core of concrete. Subsequently, lesser thermal cracking and tensile stresses are induced. The cracks that developed were curtailed by the reinforcing action of CNFs. The lack of both these mechanisms in control HSC lead to thermal cracking and subsequently complete failure in the form of spalling.
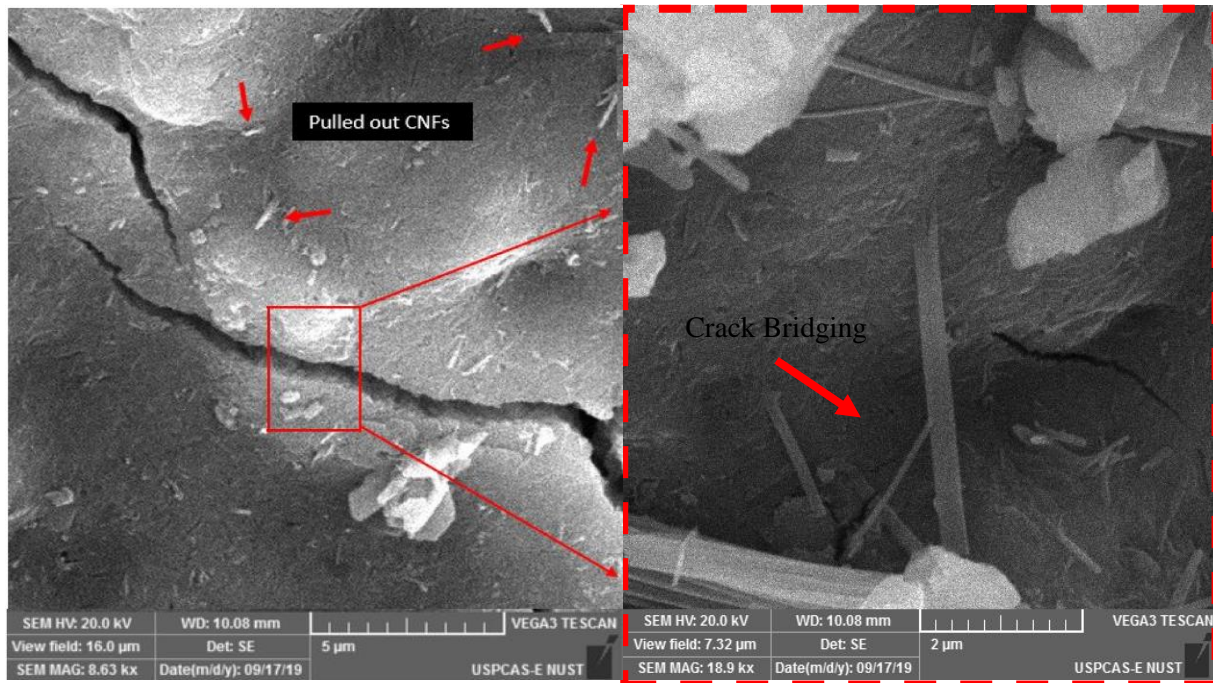
Figure 16: Crack bridging by CNFs in 0.2CNF-HSC at 600ºC

4.3.2 Compressive strength-BF-HSC

For residual test condition concrete specimens were moved to compression machine and the ultimate load at which specimens failed at various temperatures was recorded under compression. Relative and absolute residual compressive strength values as a function of temperature are presented in Fig 17. Test results shows that both type of concrete i.e. control (HSC) and modified (1B-HSC & 2B-HSC) lose compressive strength with the rise in temperature. This strength loss in compressive strength is unavoidable which is attributed to hydrothermal (loss of free and adsorbed water) and numerous physical and chemical changes that occurs in concrete matrix when exposed to high temperatures [96] . First considerable change in hydrothermal condition occurs at 100ºC which includes removal of free and adsorbed water, this causes increase in pore pressure that continues to vary up till 200ºC [12] causing loss of strength as a result of micro-cracking [97]. A considerable loss of strength occurs at 400ºC with the decomposition of calcium silicate hydrate (C-S-H) and calcium hydroxide (CH) which are the main hydrates of cement [7]. The changes above 500ºC are not only severe but unalterable [79]. Furthermore, major reason of strength degradation at 600ºC is thermal instability of aggregates as de-carbonation of limestone occurs

between 600-800°C [12]. The reduction in compressive strength due to thermal load is closely connected to characteristics of microstructure of concrete. The variation in average cylindrical strengths of modified formulations (1B-HSC & 2B-HSC) containing basalt fibers was found to be in the range of ±4% compared to compressive strengths of control formulation which shows the basalt fiber did not showed any significant improvement. However, concrete samples containing basalt fibers showed considerable resistance against spalling. For both concretes HSC and modified HSC under residual conditions, the relative residual compressive strength loss, follow a similar trend up to 200°C. However, between 200-800°C the strength degradation becomes more noticeable in control samples which ultimately spalled above 600°C. Both the modified formulation performed better in terms of strength retention at all temperatures (23-800°C) compared to the control HSC.

Similar behavior of 2B-HSC compared to 1B-HSC up to 200°C was observed. 2B-HSC outperformed 1B-HSC between 200-400°C which is attributed to the presence of significant amount of thermally resistive media in 2B-HSC compared to 1B-HSC. The presence of thermally resistive fibers in the cementitious matrices has resulted in not allowing the heat to be conducted through the concrete layers thus helped to resist against spalling and thermal stresses. 1B-HSC and 2B-HSC retained 39% and 43% while control samples retained about 32% of their strengths at 600°C. When control HSC spalled above 600°C, 1B-HSC and 2B-HSC still retained 10% and 18% of their strengths at 800°C. During testing, no spalling of modified formulation (1B-HSC & 2B-HSC) is observed due to the bridging behavior of fiber. For the modified concrete fibers served to restrain the lateral expansion of concrete and delay fracture.

Microstructural study was performed to examine the modified samples. Modified high strength concrete specimens outperformed control samples especially above 400°C. Micrograph in Fig 18 shows that crack propagation has been resisted by the crack bridging action of basalt fibers hence the presence of basalt is doubly beneficial i.e. they resist the intrusion of heat from external layers of concrete to internal layers and bridge the cracks which originates as a result of hydrothermal changes. The crack bridging nature of basalt fiber has preserved the effective load-bearing area which in turn has enhanced the strength retention. The lack of both these mechanisms in control HSC lead to thermal cracking and subsequently complete failure in the form of spalling.
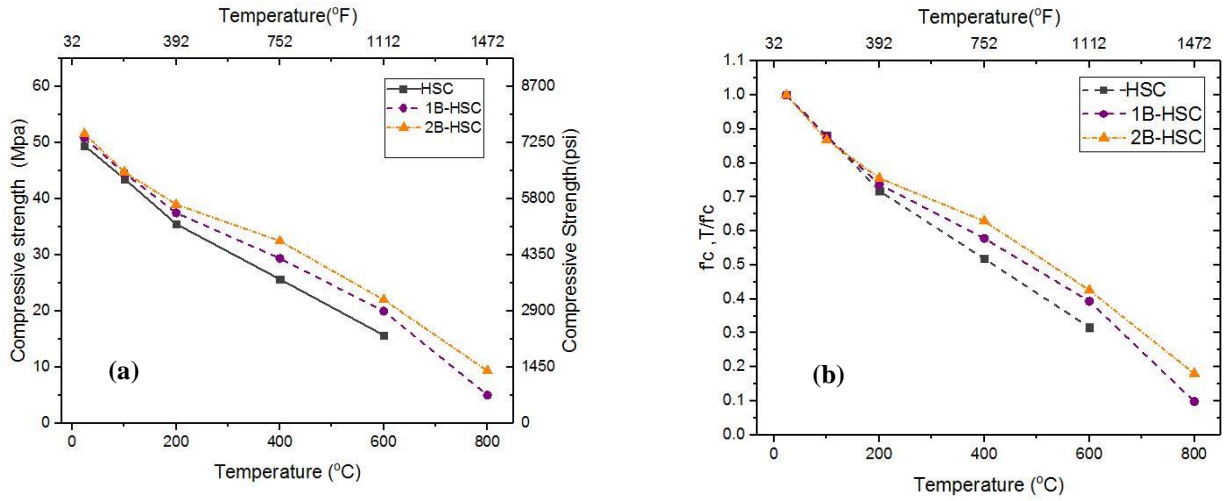
Figure 17: Variation of compressive strength as a function of temperature (a) Absolute
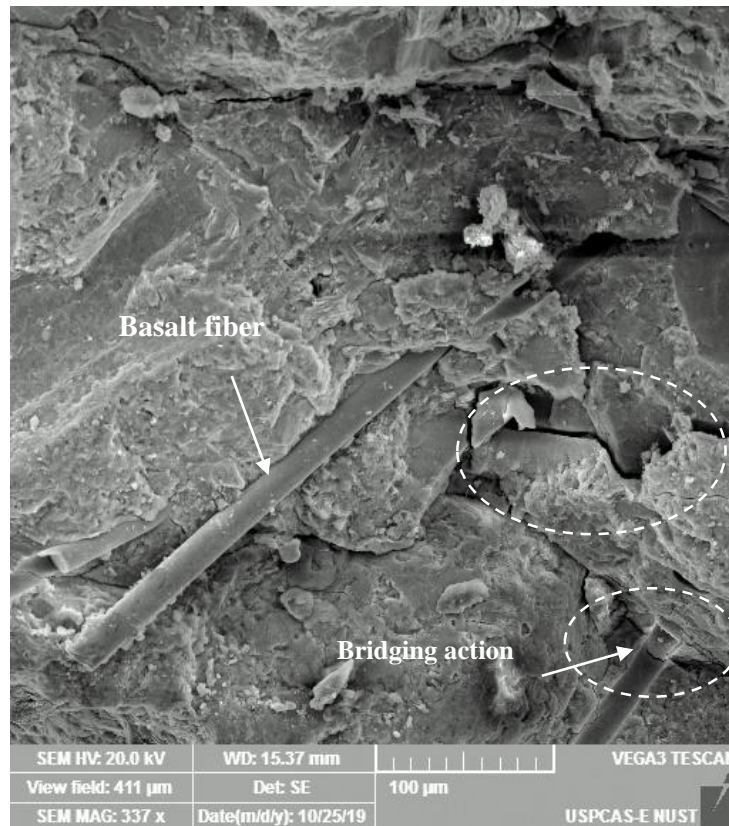
(b) Relative

Figure 18: Bridging action by BF in 2B-HSC at 600ºC

4.3.3 Tensile strength-CNF-HSC

Similar to compressive strength degradation trends, tensile strength loss occurs in all formulations which is attributed to irreversible hydrothermal, chemical and physical deterioration in the host matrices. Relative and absolute splitting tensile strength degradation trend for control and modified concrete as a function of temperature is shown in Fig 19. Initial increase in tensile strength upon nano modification for modified samples is observed, this is due to the refinement of microstructure and the presence of well dispersed CNFs inside matrix as shown in Fig 20. Similarly the uniform scatter of micro-cracks observed through visible inspection also relate to effective distribution of CNFs. The better performance and enhanced fire endurance of modified samples at elevated temperatures outperformed control samples due to crack bridging action of CNFs. As the temperature elevates, more pronounced strength loss is observed in control. Up to 200°C, no significant difference in relative tensile strength degradation of all formulations was found as control samples retained 72% compared to 0.1CNF-HSC and 0.2CNF-HSC retaining 70% and 70.2% of their relative strengths respectively. However beyond 400°C, both the modified formulations incorporated with CNFs exhibit higher relative strength retention as compared to the control formulation.

The origination, propagation and coalescing of every new crack reduces the load carrying area and this reduction in load carrying area increases the tensile stresses at critical crack tips [75]. These tensile thermal stresses increase micro-cracking in concrete matrix. In the absence of CNFs these micro-cracks widens and compromise the effective load bearing area. As observed control sample at 400°C has lost more than the half of its pristine strength (60%) which can be attributed to aforementioned reasons. However, in modified samples the higher thermal conductivity of injected CNFs helped in uniform distribution of thermal stresses. This uniformity of heat helped curb the thermal stresses that develop due to inertial effects. Secondly the crack bridging action of CNFs enabled the host matrix to further curtail these tensile cracks especially above 400°C, which is the most critical temperature for fire exposure. CNFs ensured their load transfer under tension in modified samples with their reinforcing action as shown in Fig 16 and Fig 20. At 600°C HSC lost nearly 86 % of their ambient strength while modified samples 0.1CNF-HSC and 0.2CNF-HSC lost 80% and 71% respectively highlighting their better performance.

 HSC samples were not exposed above 600°C due to risk of explosive spalling as the HSC spalled above 600°C during compressive tests. However all types of concrete exhibited higher damage

47

(higher mechanical strength loss) in tensile strength with intensification in cracking due to diametric loading than the damage in compressive strength in which some cracks tend to close-up as well. These observations are concurrent with previous studies [7]. Tensile strength degradation is more precarious than compressive strength due to the very phenomenon of increased cracking resulting from crack coalescence. The relative splitting tensile strength retention in 0.1CNF-HSC and 0.2CNF-HSC at 800°C is 12 % and 16% respectively with no spalling or major cracking observed.
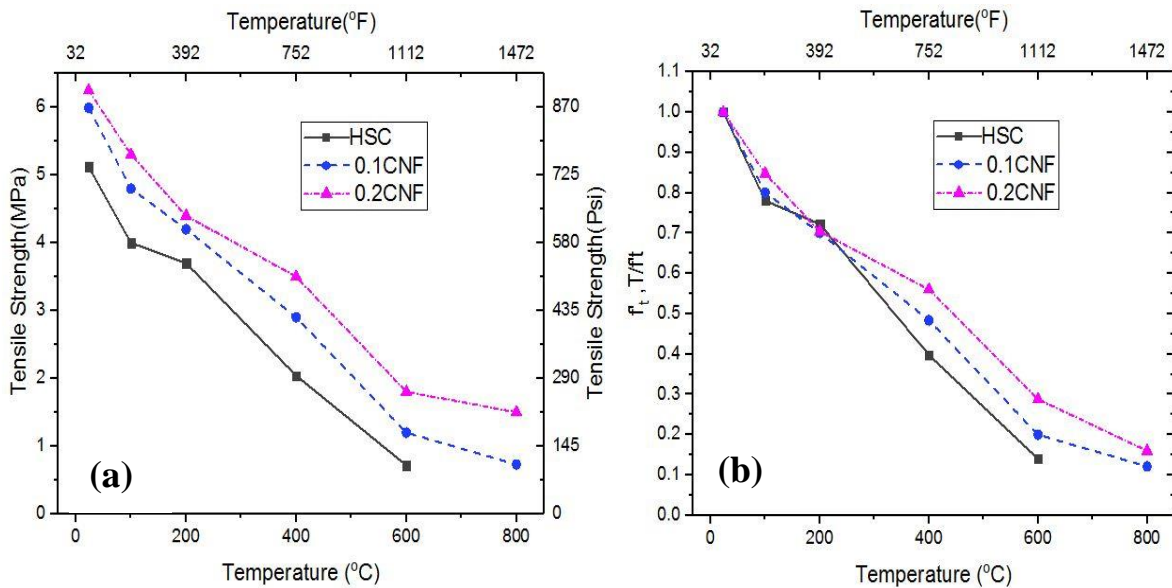
Figure 19: Variation of splitting tensile strength as a function of temperature (a) Absolute (b) Relative
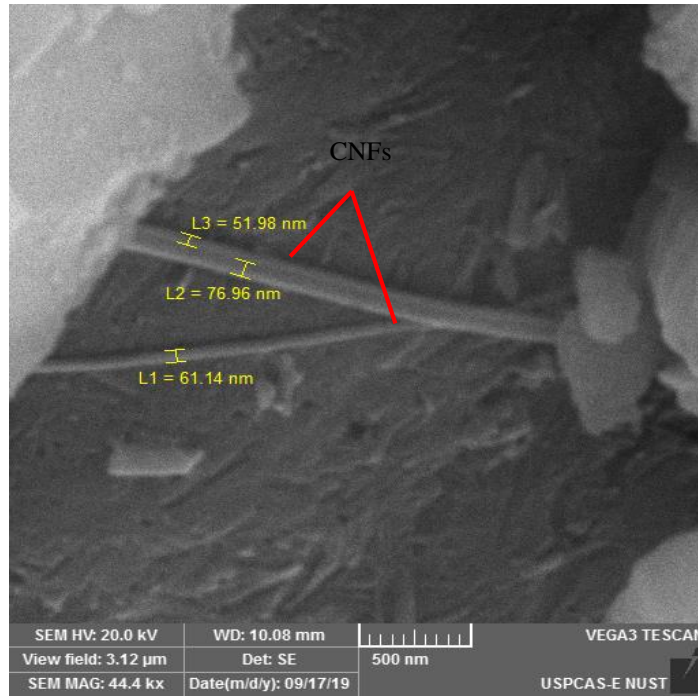
Figure 20: Well dispersed CNFs inside 0.2CNF-HSC matrix

4.3.4 Tensile strength-BF-HSC

Relative and absolute splitting tensile strength loss trend for control and modified concrete as a function of temperature is shown in Fig 21. It is observed that tensile strength loss occurs in all formulations similar to compressive strength degradation trends, which is attributed to irreversible chemical, physical and hydrothermal deterioration in the concrete matrix. Initial increase in tensile strength with the addition of basalt fibers in modified samples is observed, this is due to the higher tensile strength of basalt fibers, good adhesion between fiber and the matrix which leads to force transfer from matrix to fiber and the presence of well dispersed basalt fibers inside matrix which is evident from the SEM as shown in Fig 24. Similarly the better adhesion between fiber and matrix help resist the tensile forces via force transfer mechanism. The better performance and enhanced fire endurance of modified samples at elevated temperatures outperformed control samples due to force transfer mechanism form matrix to basalt fiber. As the fiber content increases, the splitting tensile strength of modified samples increased by about 23–34% at ambient conditions. It is mainly due to the bridging action of the well distributed basalt fiber through cracks, which effectively

restrains the propagation of micro cracks in the primary stage. As a result, the stress is transferred to the bridging fibers, and thus the development of macro cracks is delayed and the splitting tensile strength is improved. With the rise in temperature, more pronounced strength degradation is noticed in control HSC.

For residual tensile performance, significant difference in relative tensile strength degradation of all formulations was found as control samples retained 77% compared to 1B-HSC and 2B-HSC retaining 85% and 90% of their relative strengths respectively up to 200°C. However beyond 400°C, both the modified formulations incorporated with basalt fiber exhibit higher relative strength retention as compared to the control formulation. The origination and propagation of every new crack reduces the load carrying area and this reduction in load carrying area increases the tensile stresses at critical crack tips [75]. These tensile thermal stresses increase micro-cracking in concrete matrix. In the absence of basalt fiber these micro-cracks widens and reduces the effective load bearing area. As observed control sample at 400°C has lost more than the half of its primeval strength (60%) which can be attributed to aforementioned reasons. Increasing the fraction of basalt fiber in modified samples leads to a decrease in the amount of heat conducted through the thickness of concrete specimens (i.e. a decrease the thermal conductivity) at all temperature levels that lead to lower tensile strength degradation which is attributed to volumetric stability of basalt fibers against high temperature exposure [98]. Secondly the force transfer mechanism by crack bridging action between basalt fiber and the cement matrix enabled the host matrix to further restrain these tensile cracks especially above 400°C, which is the most critical temperature for fire exposure. Basalt fibers ensured their load transfer under tension in modified samples. The interface bonding between cementitious composites and aggregate is improved by the addition of fiber with their reinforcing action as shown in by micrographs Fig 24. At 600°C HSC lost nearly 86% of their ambient strength while modified samples 1B-HSC and 2B-HSC lost 77% and 66% respectively which highlights their better performance. The relative splitting tensile strength retention in 1B-HSC and 2B-HSC at 800°C is 8 % and 22% respectively with no spalling being witnessed. Fig 24 shows the SEM images of basalt fiber reinforced concretes. In this figure, bonding between basalt fibers and good adhesion between the fiber and concrete matrix with the effective dispersion of basalt fiber is observed; this bonding can lead to improved force transfer from the matrix to the fiber and an increase in the mechanical properties of the concrete.
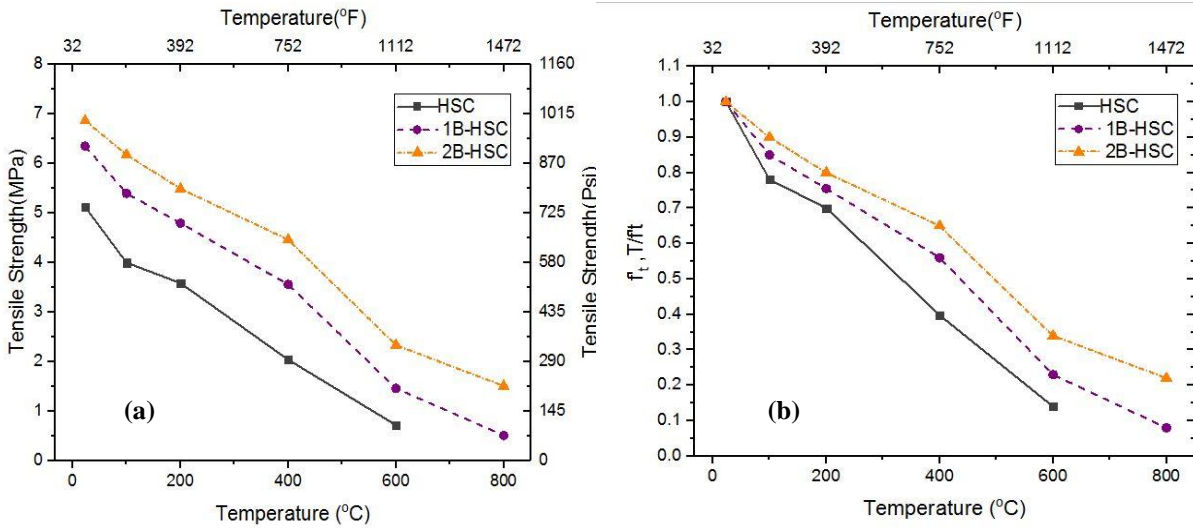
Figure 21: Variation of splitting tensile strength as a function of temperature (a) Absolute (b) Relative
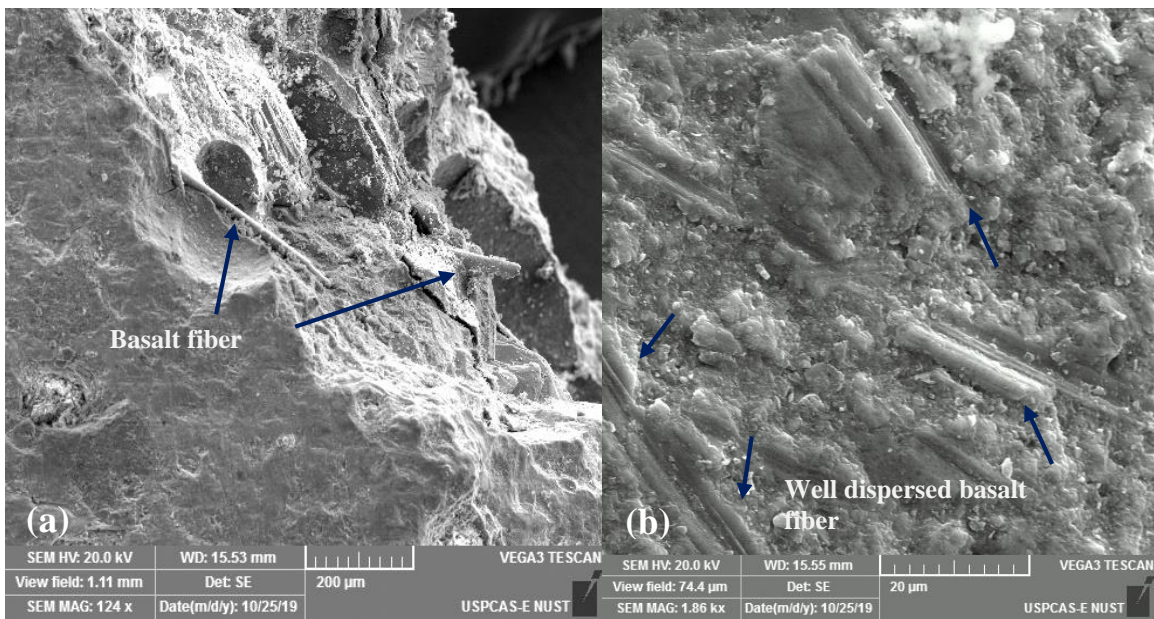

Figure 22: BF inside concrete (a) Good adhesion between matrix and BF (b) Well dispersed BFs

4.3.5 Stress-Strain response-CNF-HSC

Stress-strain response for control (HSC) and modified (0.1CNF-HSC & 0.2CNF-HSC) concrete was captured alongside the compression tests. The attached LVDTs captured even the miniscule displacements and was successful in attaining the complete load-displacements patterns till ultimate values. Trends of analyzed formulations can be seen in Fig 25. For all concrete types the obtained data reveals that the increase in temperature results in a decrease in the ultimate peak stress with a subsequent increase in the corresponding peak strain at all target temperatures. This behavior is typical for concrete at elevated temperatures for stress-strain response which is attributed to microstructural deterioration [99]. Expulsion of water from matrix leads to dehydration and development of cracks. These cracks reduce the effective load bearing area which in turn reflects in higher strain. Bond disintegration due to aggregate-paste thermal incompatibility and subsequent thermal creep also plays an important role in the characteristic pattern of fire exposed concrete [12]. Decomposition of hydrates especially calcium hydroxide (CH) and de-carbonation of calcium carbonate which is the major chemical constituent of limestone aggregates causes major cracking [73]. These deteriorations when acting together badly influence the concrete matrix and compromise its structural integrity. Such deterioration were observed when microstructure of control HSC sample was analyzed using scanning electron microscopy. Micrographs attached in Fig 26 show a deteriorated microstructure with amorphous hydration products. The peak strains for The peak strains for control HSC were 39%, 82 %, 167% higher to their ambient strains after exposure to 200, 400, 600°C. Similar pattern was observed in modified concretes containing nanofibers. The strains increased 38%, 90%, 181%, 206% and 42%, 117%, 184%, 274% relative to their ambient strains after exposure to 200, 400, 600, 800°C for 0.1CNF-HSC and 0.2CNF-HSC respectively. However, the peak residual strain in case of 0.1CNF-HSC and 0.2CNF-HSC at 600 °C are 13% and 23% higher compared to that of control HSC respectively. This indicates towards a ductile behavior of CNFs reinforced matrices and improved strength

retaining ability under fire conditions. This can attributed to preservation of effective load bearing area by crack bridging action by CNFs as evident in Fig 16 and Fig 20.
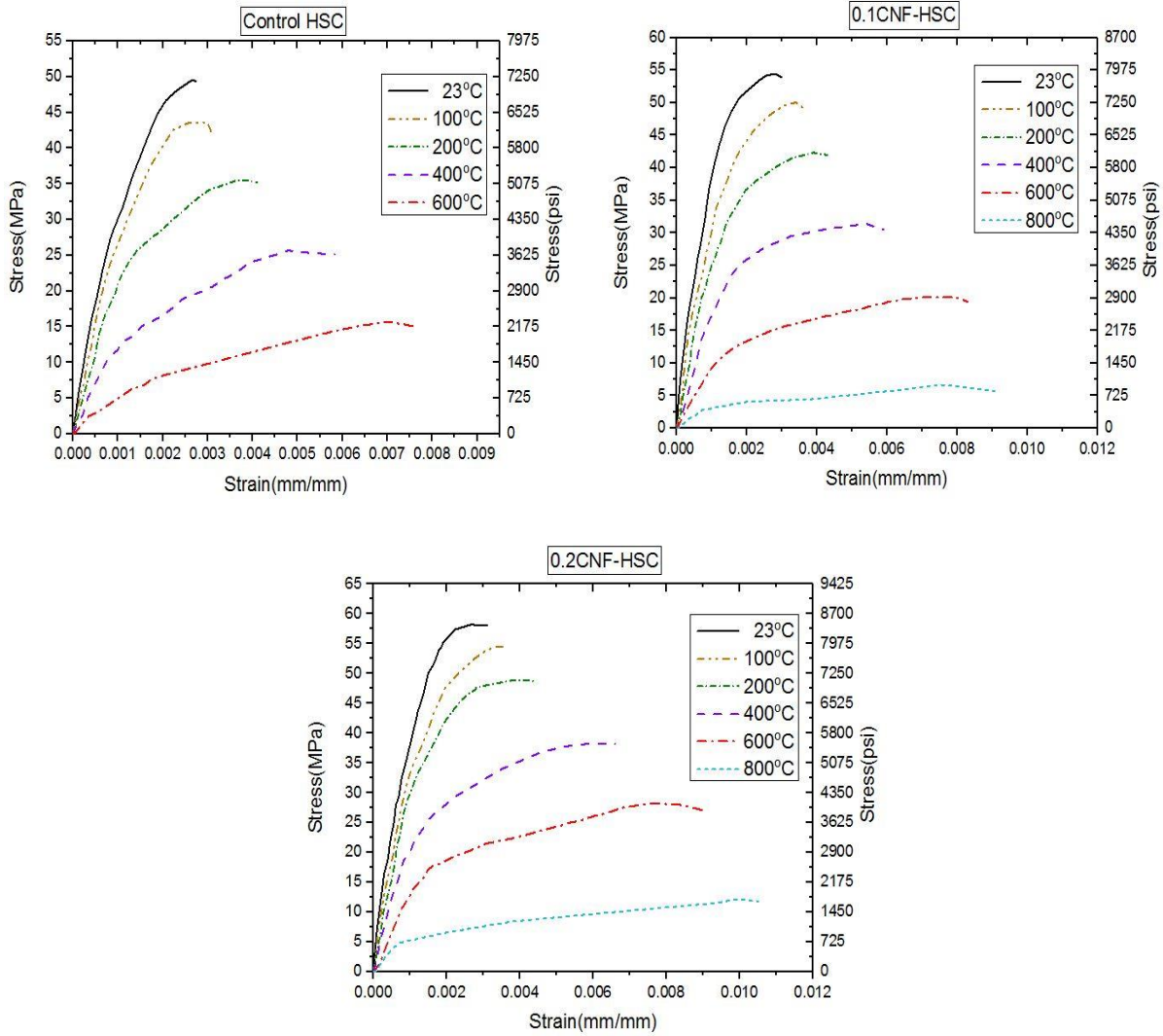

Figure 23: Residual stress–strain behavior of (a) Control HSC (b) 0.1CNF-HSC (c) 0.2CNF-HSC at various temperatures
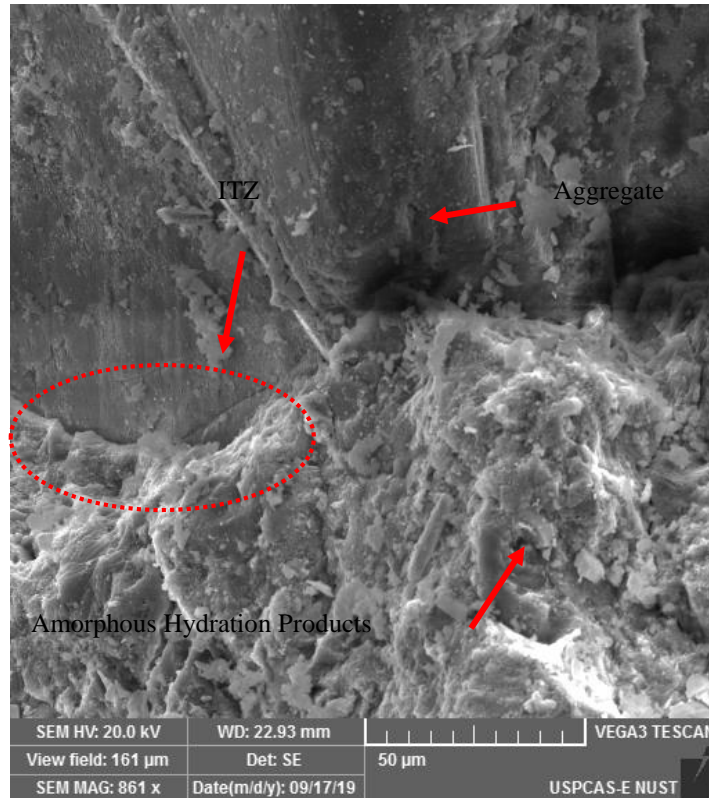
Figure 24: Deterioration of microstructure of control
HSC at 600ºC

4.3.6 Stress-Strain response-BF-HSC

Stress-strain response for control (HSC) and modified (1B-HSC & 2B-HSC) concrete was obtained through prescribed test procedure earlier at each target temperature for all the formulations under compression. The attached LVDTs captured the complete load-displacements patterns till ultimate values and was successful in attaining even the miniscule displacements. Trends of analyzed formulations can be seen in Fig 27. For all concrete types the obtained data reveals that the increase in temperature results in a decrease in the ultimate peak stress with a subsequent increase in the corresponding peak strain at all target temperatures. This behavior is typical for concrete at elevated temperatures for stress-strain response which is attributed to microstructural deterioration [99]. Expulsion of water from matrix leads to dehydration and development of cracks. Decomposition of hydrates especially calcium hydroxide (CH) and de-carbonation of calcium carbonate which is the major chemical constituent of limestone aggregates causes major cracking [73]. These deteriorations when acting together badly influence the concrete matrix and compromise its structural integrity. Such deterioration were observed when microstructure of control HSC sample was analyzed using scanning electron microscopy.

Micrographs attached in Fig 26 show a deteriorated microstructure with amorphous hydration products. The plot of stress-strain curves for modified formulations showed that the addition of basalt fibers enhances the ductile behavior of the concrete. The values of the strains of the control mix was found to be the lowest among all the mixes at all temperatures. This indicates that basalt fibers were fully active and showed resistance against extensive cracking of concrete. With the increasing dosage of fiber, the resistance against cracking was also increased; therefore, the modified specimen attained higher strain values. The peak strains for control HSC were 38%, 82 %, 167% higher to their ambient strains after exposure to 200, 400, 600°C. Similar pattern was observed in modified concretes containing basalt fibers. The strains increased 51%, 110%, 182%, 233% and 52%, 114%, 191%, 251% relative to their ambient strains after exposure to 200, 400, 600, 800°C for 1B-HSC and 2B-HSC respectively. However, the peak residual strain in case of 1B-HSC and 2B-HSC at 600 ^{o}C are 33% and 44% higher compared to that of control HSC respectively. This indicates towards a ductile behavior of basalt fiber reinforced matrices and improved strength retaining ability under fire conditions. This can attributed to preservation of effective load bearing area by crack bridging action by basalt fibers as evident in Fig 18 and Fig 24. Basalt fiber reinforced concrete included higher energy absorption capacity after attaining the optimum load which resulted in increased ductility.
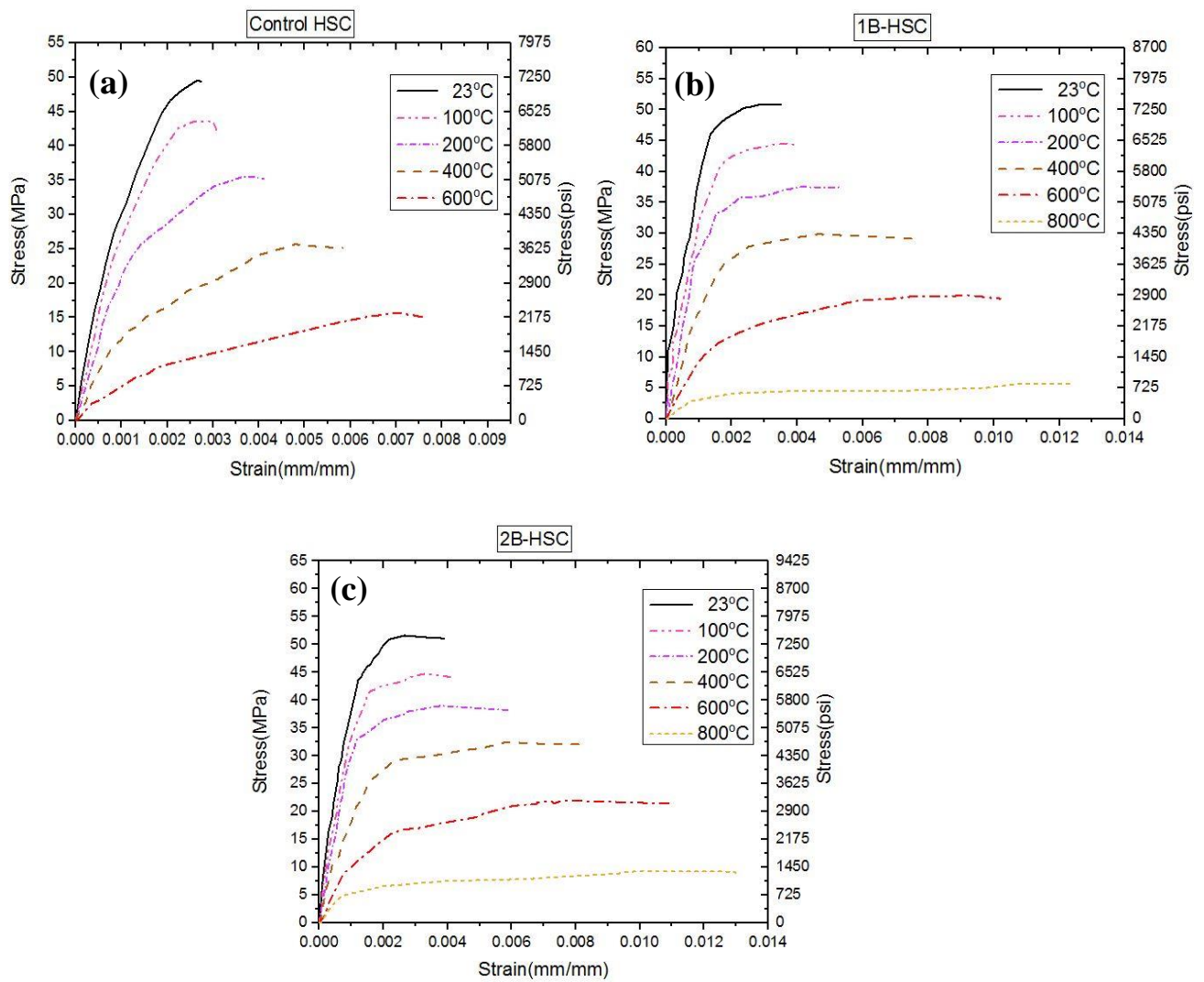
Figure 25: Residual stress–strain behavior of (a) Control HSC (b) 1B-HSC (c) 2B-HSC at various temperatures

4.3.7 Elastic Modulus-CNF-HSC

Compressive stress-strain data is utilized to calculate elastic modulus (E) for HSC and modified (0.1CNF-HSC & 0.2CNF-HSC) concrete using expression proposed by ASTM C469 [95]. Strains corresponding to 40% of stress value are considered to contemplate the elastic moduli. The variation of absolute (E_T) and relative (E_T/E) elastic modulus loss is shown in Fig 28. A 17% and 21% average increase is observed in 0.1CNF-HSC and 0.2CNF-HSC due to nano-modification at ambience. It is evident from elastic modulus degradation that retention of modulus is higher and relative loss is lower in case of modified samples especially in the range of 400-800°C owing to the presence of nano-reinforcements and their reinforcing action. It was expected because these mixes were experiencing lesser loss in compressive strength and showed ductile behavior in comparison to the control specimen. In addition to that, when control HSC could not sustain exposure above 600°C due to thermally induced spalling,

modified sample retained 9% and 17% of elastic modulus for 0.1CNF-HSC and 0.2CNF-HSC at 800ºC respectively. This also confirms that control high strength concrete (HSC) which exhibits higher loss in mechanical strengths will also exhibit more relative loss in elastic modulus [100]. 0.1CNF-HSC and 0.2CNF-HSC lost 51% and 45% elastic modulus at 400ºC compared to control lost 62%. The enhanced performance of modified samples is attributed to effective preservation of load bearing area by crack bridging action of nano-reinforcements as evident in micrographs shown in Fig 16 and Fig 20. Similarly, the effective distribution of thermal stresses and the reduction of thermal inertia due to thermally conductive nature of CNFs assist in strength retention. The uniform scatter of cracks as evident by the visual inspection (Table 9) upholds the claim for uniform thermal stress distribution.
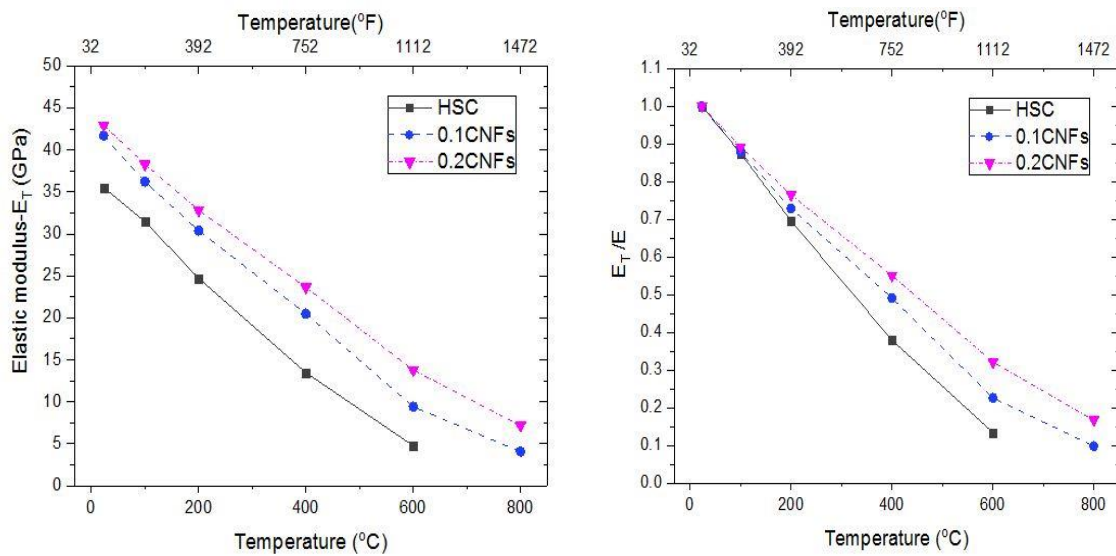
Figure 26: Variation of elastic modulus as a function of temperature (a) Absolute (b) Relative

4.3.8 Elastic Modulus-BF-HSC

Compressive stress-strain curves at elevated temperatures is used to calculate elastic modulus (E) for HSC and modified (1B-HSC & 2B-HSC) concrete using the expression as per ASTM C469 [95]. Calculated values of secant modulus correspond to stress equal to 40% of peak compressive strength at a temperature. Strains corresponding to 40% of stress value are considered to calculate the elastic moduli. The variation of absolute (E_T) and relative (E_T/E) elastic modulus loss is shown in Fig 29. An 8% and 22% average increase is observed in 1B-HSC and 2B-HSC due to basalt fiber modification at ambience. The presence of basalt fibers increased the strain capacity of modified formulations thus, leading to more energy absorption. Elastic modulus degradation results shows that retention of modulus is higher and relative loss

is lower in case of modified samples owing to the presence of basalt fibers. It was expected because these mixes were experiencing lesser loss in compressive strength and showed ductile behavior in comparison to the control specimen. Further, when control HSC could not sustain exposure above 600°C due to thermally induced spalling, modified sample retained 4% and 18% of elastic modulus for 1B-HSC and 2B-HSC at 800°C respectively. This is also in conformity with previous research [100] that control high strength concrete (HSC) which exhibits higher loss in mechanical strengths will also exhibit more relative loss in elastic modulus . 1B-HSC and 2B-HSC lost 57% and 46% elastic modulus at 400°C compared to control lost 63%. The enhanced performance of modified samples is attributed to effective preservation of load bearing area by enhanced interlocking and better adhesion between basalt fibers and cement matrix as evident in micrographs shown in Fig 18 and Fig 24.
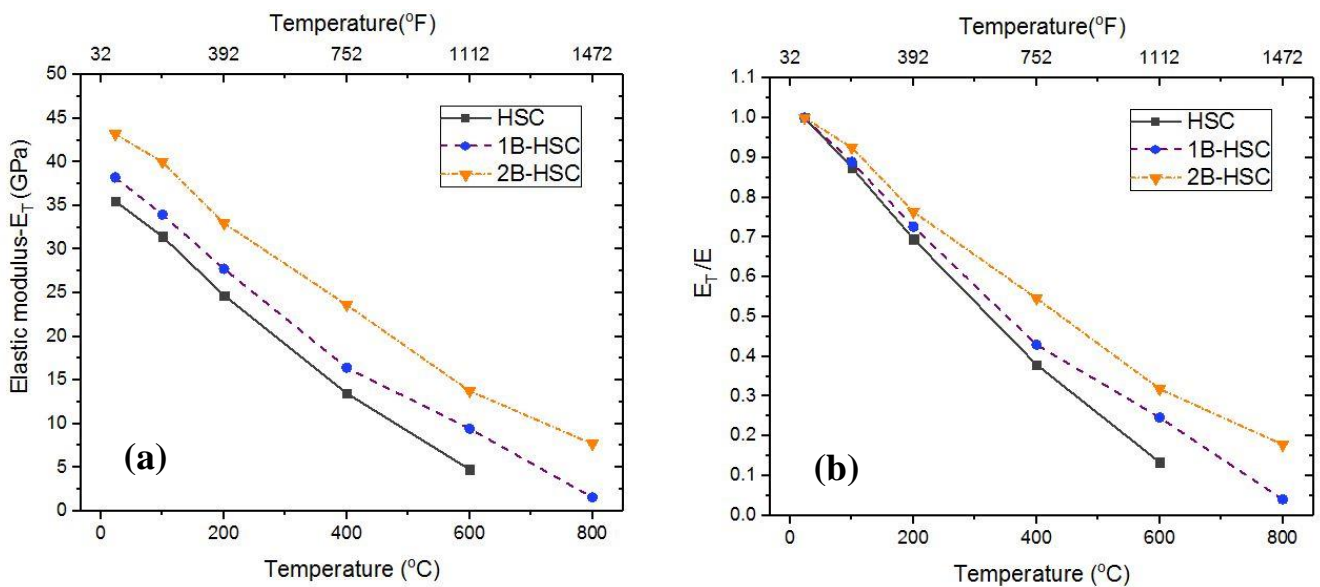
Figure 27: Variation of elastic modulus as a function of temperature (a) Absolute (b) Relative

4.3.9   Compressive toughness (T$_C$)-CNF-HSC

Area under stress-strain curve is used to calculate compressive toughness (T$_C$) which explains the energy absorbed by the specimen before failure and predicts its capacity to resist deformation under compression. The study of toughness also helps to better interpret the results of load-deformation curves. The data obtained from stress-strain response point toward the samples containing CNFs tend to rupture at greater strains and fracture at higher stresses. To calculate the increment in the fracture energy of all analyzed formulations compressive toughness (T$_C$) was evaluated against exposure temperature as shown in Fig 30. For effective interpretation of increase in energy absorption by modifies samples containing CNFs,

58

toughness index (TI) is used [45]. The values of attained TI are presented in Fig 30. Percentage relative increase in toughness of modified samples compared to control is explained by a base line. The baseline represents the energy dissipated by the control (HSC) specimens.

$$TI= \frac{\text{Tc of modified specimen at a particular temperature}}{\text{Tc of control specimen at that particular temperature}}$$
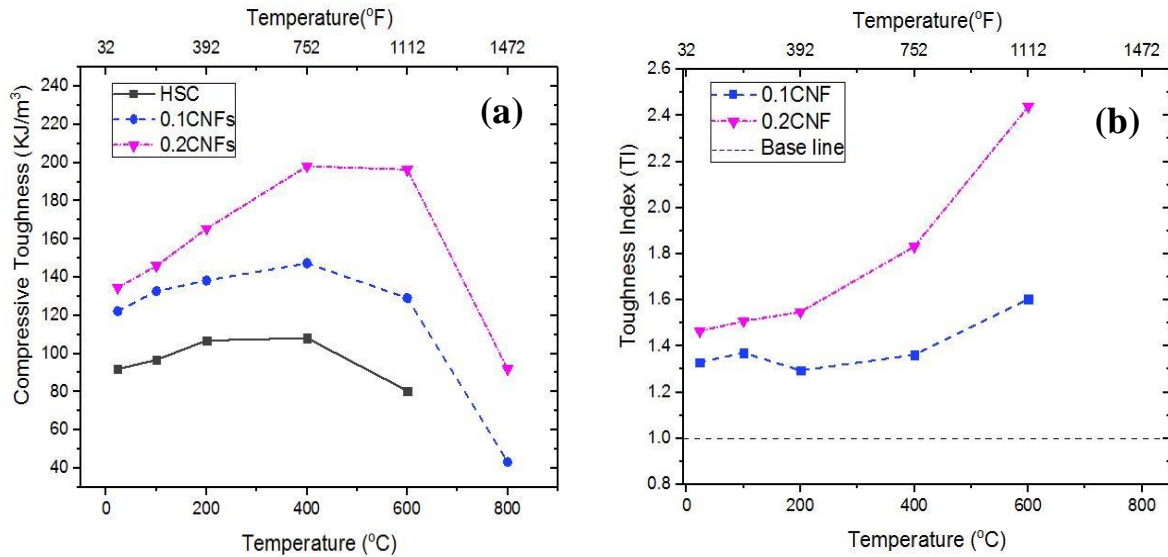

Figure 28: Variation of Compressive toughness and toughness index of concrete samples (a) Compressive toughness (b) Toughness index

Massive 33 to 60% and 46 to 143% increase in toughness energy has been observed in modified samples (0.1CNF-HSC and 0.2CNF-HSC) with maximum gain occurring at 600°C, 60% and 143% respectively. At 400°C, the relative increase in toughness energy is found to be 36% and 83% in 0.1CNF-HSC and 0.2CNF-HSC compared to control. While at 600°C increase is 60% and 143% respectively. This increase in toughness of modified concrete is attributed to lateral restraint provided by inter-particle reinforcing action due to bridging effect of CNFs against the initiation and propagation of cracks. Values of toughness index indicates towards enhanced fracture and deformability characteristics. Improved toughness energy capacity of modified samples at elevated temperatures which can be advantageous for relieving the fire induced spalling in reinforced concrete members so was observed in this study as well. The improved energy absorption capacity and tensile capacity of this modified concrete may well make it suitable for application in very specialized industry such as nuclear, gas, power and oil.

4.3.10 Compressive toughness (T_C)-BF-HSC

Compressive toughness (T_C) explains the energy absorption capacity of the specimen before failure and predicts its capability to resist deformation under compression. Area under stress-strain curve is used to calculate T_C. The data obtained from stress-strain response point toward

the samples containing basalt fibers tend to rupture at greater strains and fracture at higher stresses. To calculate the increment in the fracture energy of all analyzed formulations compressive toughness (T_C) was evaluated against exposure temperature. Toughness index (TI) is introduced for effective interpretation of increase in energy absorption by modifies samples containing basalt fibers [45]. The values of attained TI are presented in Fig 31. Percentage relative increase in toughness of modified samples compared to control is explained by a base line. The baseline represents the energy dissipated by the control (HSC) specimens.

$$TI = \frac{Tc \text{ of modified specimen at a particular temperature}}{Tc \text{ of control specimen at that particular temperature}}$$

Trend represents that massive 49 to 105% and 71 to 144% relative increase in toughness energy has been observed in modified samples (1B-HSC and 2B-HSC) with maximum gain occurring at 600°C, 105% and 144% respectively. At 400°C, the relative increase in toughness energy is found to be 76% and 109% in 1B-HSC and 2B-HSC compared to control. While at 600°C increase is 105% and 144% respectively. This increase in toughness of modified concrete is attributed to force transfer mechanism from matrix to basalt fiber, better adhesion between fiber and matrix and higher energy absorption capacity of basalt fibers against the initiation and propagation of cracks as evident by micrographs in Fig 32. Values of toughness index indicates towards enhanced fracture and ductility characteristics. Improved toughness energy capacity of modified samples at elevated temperatures which can be advantageous for relieving the fire induced spalling in reinforced concrete members so was observed in this study as well.
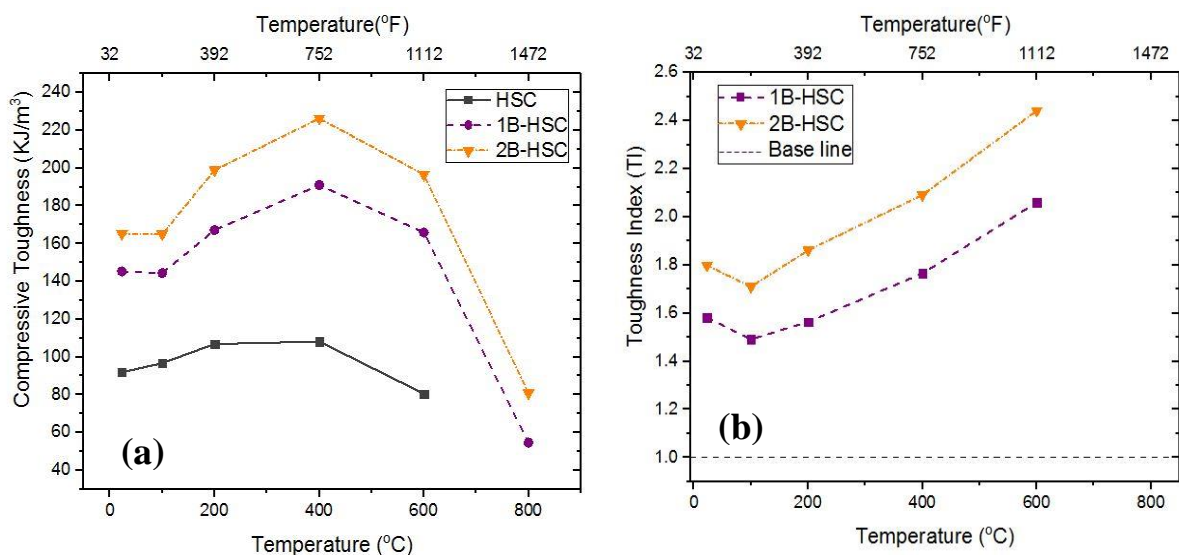

Figure 29: Variation of Compressive toughness and toughness index of concrete samples (a) Compressive toughness (b) Toughness index
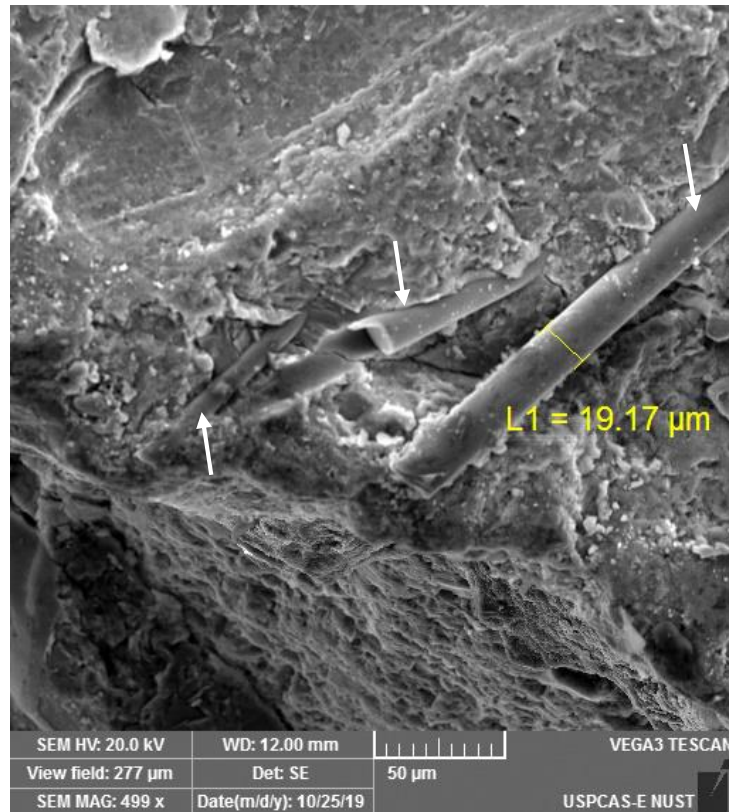
Figure 30: Force transfer mechanism in 2B-HSC at
600ºC

4.3.11 Mass loss-CNF-HSC

Mass loss in concrete helps to quantify the porosity, presence of moisture in the form of free, absorbed, capillary, both adsorbed and chemically coalesce water in the matrix [68]. With the increase in temperature, the ratio of mass loss provides an assessment of progressive deterioration and microstructure damage. Decomposition of hydrates and removal of water form concrete matrix are major contributors in mass loss [101]. The binding matrix in concrete has a strong relationship between residual strength and mass loss owing to moisture disturbances as mix water plays key role in concrete's gain in strength, so does moisture removal in dehydration affects the loss in strength and deterioration of concrete matrix. As the temperature increases, so does the moisture loss. The differential rates depend upon microstructure density, hydro-thermal processes, and bonding condition of water present in concrete [102]. Mass loss (M_T/M) results for HSC and modified (0.1CNF-HSC & 0.2CNF-HSC) concrete under residual condition as a function of temperature are shown in Fig 33. It is observed that the unit weight of all analyzed formulations decrease upon exposure to fire. Mass loss up to 100ºC can be associated to the fact that phase change of moisture from liquid to vapor takes place in this range. The mass loss up to 200ºC follows an in differentiable pattern. However, high strength concretes modified with CNFs show a lesser mass loss in the range of

200-800°C compared to control sample. This lesser mass loss in reinforced samples is attributed to the increased amount of C-S-H gel. CNFs have the capacity to act as nucleation sites and provide an assistive environment for hydrates to grow stably [83]. The observation of reduced mass loss in case of nano-modified concrete, is in line with previous studies by Waqas et.al [45]. The author argued that the nano-media establishes potential areas of interaction with hydration products of cements, which allows the presence of metastable states of liquid water over wider temperature ranges [103]. Thus a high stiffness C-S-H gel is produced as a result of nano-intrusion which also improves its potency against fire. High stiffness C-S-H gel is evident by micrograph shown in Fig 34.
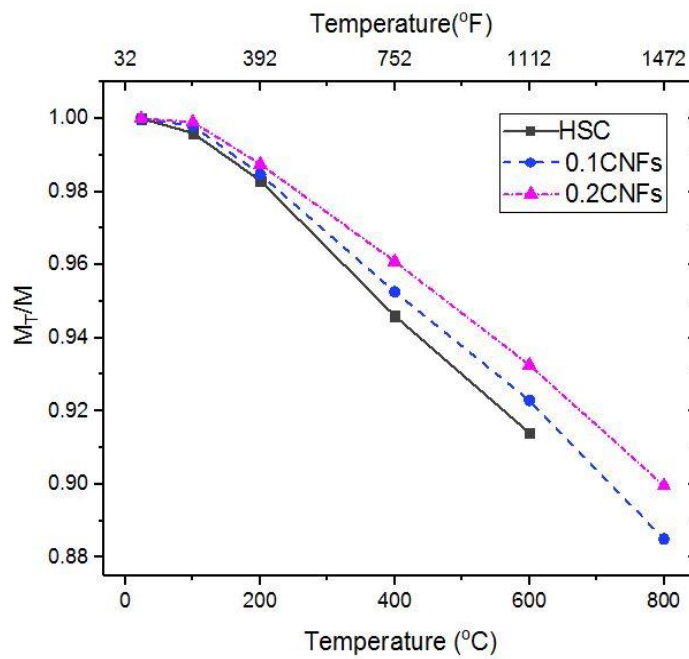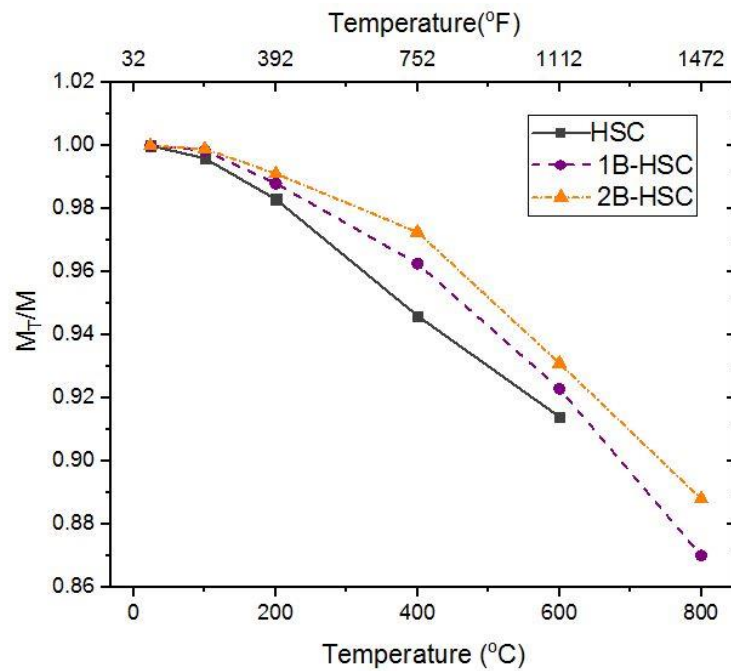

Figure 31: Mass loss as a function of temperature
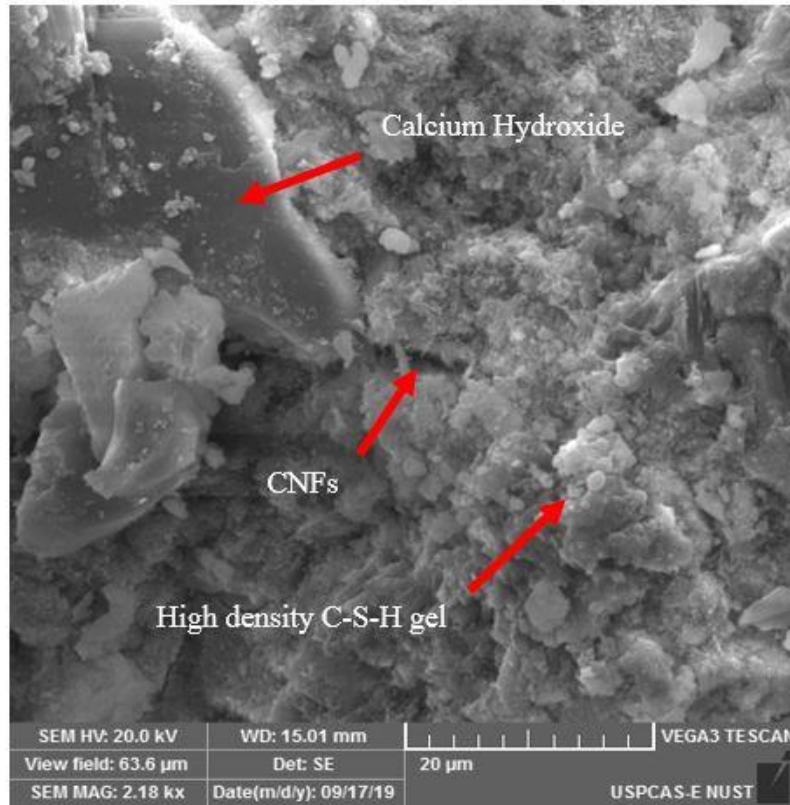
Figure 32: High C-S-H gel in 0.2CNF-HSC

4.3.12 Mass loss-BF-HSC

Mass loss (M_T/M) results for HSC and modified (1B-HSC & 2B-HSC) concrete under residual condition as a function of temperature are shown in Figure 35. It is observed that the unit weight of all analyzed formulations decrease upon exposure to fire. Due to phase change of moisture from liquid to vapor mass loss occur at 100°C. The mass loss up to 200°C follows an in differentiable pattern. However, high strength concretes modified with basalt fiber show minute loss of mass in temperature range of 200-800°C compared to control sample. BF not only preserved its physical shape but also have not lost the mechanical integrity at 800°C. This lesser mass loss in modified samples is attributed to the increased amount of nucleation sites which is because of the intrinsic property of the basalt rocks which nucleates at high temperature [33]. Heat resistance and higher thermal stability of BF is because of the intrinsic material feature of natural basalt rocks that has a capability to form nucleation site at high temperatures [104]. The key element decisive of high temperature stability of BF is due to their behavior of crystallization. In addition to that, owing to higher percentage of iron oxides in BF rock, its crystallization initiates with the spinal structure phase due to ferrous cations oxidation in fiber surface. With the temperature elevation the pyroxene crystallization take place on spinal crystals that ultimately act as nucleation sites [105].

This can also be attributed to addition of basalt fiber that tips towards a decrease the thermal conductivity that caused lower amount of heat conducted through the thickness of concrete specimens which is due to the volumetric stability of BF at high temperature condition [98] thus, causing lower mass loss in modified formulation. The authors are of the view that the basalt fiber improves potency of modified specimens against fire as the stability of basalt fiber in concrete matrix at elevated temperatures is witnessed by SEM micrograph as shown in Figure 36.

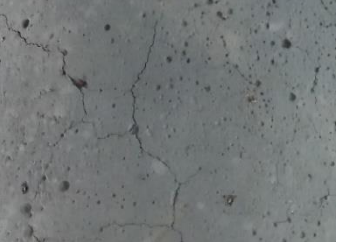Figure 33: Mass loss as a function of temperature
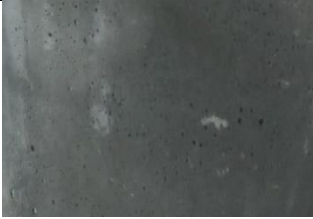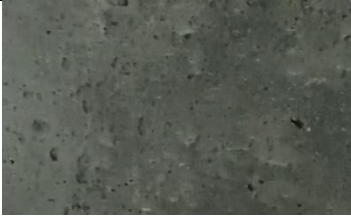
Figure 34: Amorphous hydration products and
fiber pull out 2B-HSC at 800ºC

4.3.13 Visual assessment of CNF-HSC specimens

Preliminary visual inspection is performed to identify the fire damage. It is important to observe the damaged structure by conducting a comprehensive analysis and building certain interpretations about the degree of the fire, e.g. noticeable degradation, magnitude and spread pattern of the fire etc. [106]. Macrostructure of concrete that is visible to unaided human eye is gross surface texture of concrete specimen. The visual inspection of control and modified HSC exposed to 23-800ºC shows the presence of localized cracks as presented in Table 9. However cracks were uniformly distributed and lesser cracking was observed in modified samples compared to the control sample which spalled between 600-800ºC that no significant cracking was observed in any formulation between 23-200ºC which is attributed to lesser disintegration of aggregate-paste bond and lower severity of thermal gradient between core and surface of the specimens. Above 200ºC cracking was observed in control HSC which is attributed to dense microstructure which does not allow easy release of pore pressure and is prone to cracking. However, no such cracking was observed in the modified samples. Intense spalling was observed in control specimen after 600ºC while minor cracks are observed in the modified specimens. The extent of cracking in 0.2CNF-HSC was less compared to 0.1CNF-HSC. The presence of significant amount of nano media in 0.2CNF-HSC has assisted the concrete matrix to homogeneously disperse thermal stresses (main cause of thermal cracking). Color changes in concrete after exposure to high temperature also help identify the severity of fire to which it has been exposed. Further, it provides useful information while establishing serviceability of a reinforced concrete structure after a fire event. The visual inspection of concrete samples showed no major color change till 200ºC. In modified samples, at temperatures of 400ºC and above, major changes in the color are observed. This color change is changed from light gray at 400ºC to light pink at 600ºC, and Gainesboro gray at 800ºC. These changes in color are conforming to the literature and further strengthen the claim that CNFs chemically compliment the host matrix [107].

Table 9: Visuals for color changes, cracking of reference and modified HSC at ambient and elevated temperature conditions
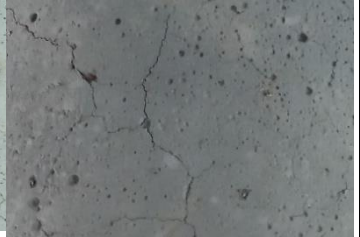
Temp (°C)	0.2CNF-HSC	0.1CNF-HSC	HSC
200			
400			
600			
800			Specimen spalled below 800°C

4.3.14 Visual assessment of BF-HSC specimens

At first, visual assessment is performed to categorize the damage caused by elevated temperature. It is decisive to observe the damaged structure by performing a comprehensive analysis and building definite interpretations about the degree of the fire, e.g. apparent degradation, crack pattern and degree of disintegration caused by fire [106].

Macrostructure of concrete that is noticeable to unassisted human eye is gross surface texture of concrete sample. The visual examination of both control and modified HSC exposed to 23-800°C indicates the existence of localized cracks as presented in Table 10. However, lesser cracking was observed in basalt fiber reinforced samples as the cracks were uniformly distributed compared to the control HSC which spalled between 600-800°C. Because of lesser disintegration of aggregate-paste bond and lower severity of thermal gradient between core and surface of the specimen, insignificant cracking was observed in all formulations within the temperature range of 23-200°C as presented in Table 10. Thermal cracking was observed in control formulation above 200°C which is attributed to highly dense microstructure of concrete matrix which does not allow easy release of pore pressure and is vulnerable to cracking. Nonetheless, modified samples showed resistance to such cracking as no cracks were produced on the macrostructure. Control HSC showed intense spalling above 600°C whereas minor cracks were observed in the fiber reinforced specimens. The vicinity of cracking in 2B-HSC was less compared to 1B-HSC. The ubiety of significant amount of basalt fibers inside concrete matrix efficaciously facilitated to resist thermal stresses of tensile nature. Color changes in concrete after being exposed to elevated temperatures also help distinguish the sternness of fire to which it has been exposed. Additionally, it yields handy information while establishing serviceability of a reinforced concrete structure after a fire event. The visual inspection of concrete samples showed no major color change till 200°C. In modified samples, at temperatures of 400°C and above, major changes in the color are observed. This color change is transformed from light gray at 400°C to dark gray at 800°C.

Table 10: Visuals for color changes, cracking of reference and modified HSC with basalt fiber at ambient and elevated temperature conditions

Temp (°C)	1B-HSC	2B-HSC	HSC
200			
400			
600			
800			Specimen spalled below 800°C

4.3.15 Ultrasonic Pulse Velocity Measurement-CNF-HSC

Ultrasonic pulse velocity (UPV) test is a non-destructive procedure that is applied to detect internal defects in concrete. To evaluate homogeneity and to indicate presence of voids or cracks in the concrete, velocity of longitudinal waves through the concrete matrix are measured [108, 109]. In addition to that, these ultrasonic measurements are a remarkable tool to evaluate the residual stiffness in concrete member affected by high temperature [110]. In this study, UPV tests are performed according to the procedures prescribed in ASTM C597 [111]. A testing apparatus consisting of an amplifier, a couple of transducers, a pulse generator, a time measuring circuit, along with connecting cables is used. The measured UPV values are presented in Fig 37 which depicts that the UPV values of specimen exposed above ambient temperatures (100-800°C) were lesser compared to the unheated specimens. This observation

compliments the well-established literature [112]. Handoo et al. experimentally witnessed UPV values reduction from 4.05 to 0.33 km/s with the increase in temperature from 100-700°C [112]. The decrease in UPV values is often attributed to irreversible hydro-thermal changes occurring in concrete matrix when it is exposed to elevated temperatures [79]. Modified formulations (0.1CNF-HSC & 0.2CNF-HSC) showed comparatively higher UPV values at elevated temperatures than control samples. This is mainly due to the better cross-sectional area retention and lesser damage to microstructure as evident by microstructural analysis shown in Fig 16 and 20. Though HSC spalled well before 800°C, 0.1CNF-HSC and 0.2CNF-HSC still showed average UPV values of 0.9 km/s and 1.7 km/s respectively.
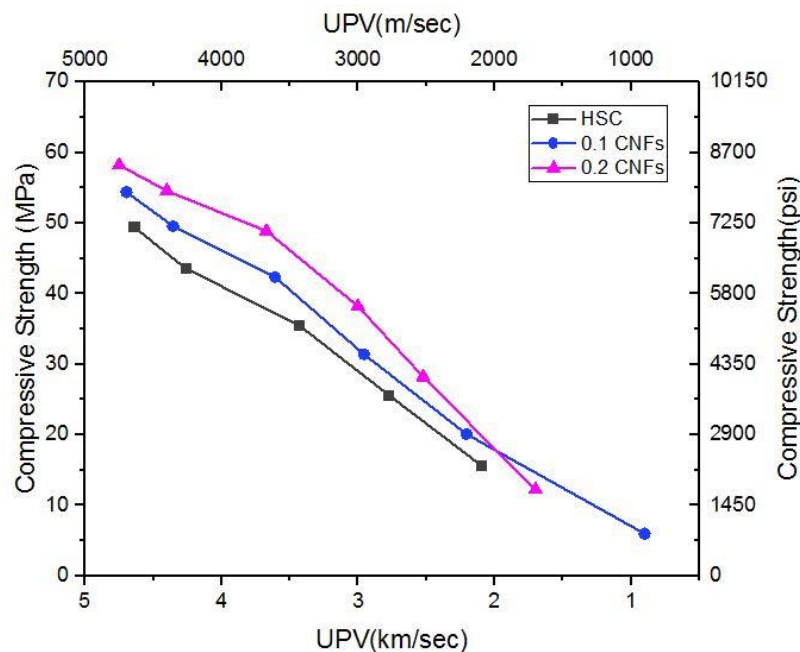
Figure 35: Compressive strength vs. UPV values

4.3.16 Mathematical Relationships-CNF-HSC

Mathematical equations have been developed to determine the response of fire-damaged reinforced concrete structural members for future computational use. Relationships for properties such as mechanical strength (tensile and compression), associated parameters such as elastic modulus and toughness have been derived. Furthermore, similar relationships for durability parameters such mass loss and UPV of modified formulations that cover the entire exposure range of 23–800°C are presented. These sets of mathematical equations, based on literature [102, 113] can help quantify the residual performance of concrete members exposed to fire. A commercial statistical software, Minitab [114] was utilized to perform regression

analyses to contemplate these empirical relationships. For every statistical model, material property is selected as response factor while temperature is taken as the predictor parameter. The validation of any statistical models is projected by coefficient of determination R^2 which determines the precision of any model, with 100% reflecting full accuracy.

For both the modified formulations (0.1CNF-HSC & 0.2CNF-HSC), the value of R^2 lied in between 87% to 98%, which shows good coherence. The relationship between material property degradation and exposure temperature can be related using a coefficient β_T. The values of β_T for elastic modulus, tensile strength, compressive strength, toughness, mass loss and UPV are estimated for the modified samples (0.1CNF-HSC & 0.2CNF-HSC), and are presented in Table 11. At different temperatures, coefficient β_T can be utilized for calculating mechanical and durability properties. These mathematical equations can be helpful to predict performance of CNFs reinforced HSC under fire conditions in future analytical studies.

Table 11: Relationship between material property and temperature-CNF-HSC

Formulation Type	Property relationships
0.1CNF-HSC	$\beta_{T,\,compression} = \left\{ \begin{array}{ll} 1 & 23°C \\ 1.0213 - 0.001122T & 100°C \leq T \leq 800°C \end{array} \right\}$
	$\beta_{T,\,Tensile} = \left\{ \begin{array}{ll} 1 & 23°C \\ 0.9487 - 0.001124T & 100°C \leq T \leq 800°C \end{array} \right\}$
	$\beta_{T,\,Elastic\ Modulus} = \left\{ \begin{array}{ll} 1 & 23°C \\ 0.9857 - 0.00117T & 100°C \leq T \leq 800°C \end{array} \right\}$
	$\beta_{T,\,Toughness} = \left\{ \begin{array}{ll} 1 & 23°C \\ 1.2821 + 0.000416T & 100°C \leq T \leq 600°C \end{array} \right\}$
	$\beta_{T,\,Mass\ loss} = \left\{ \begin{array}{ll} 1 & 23°C \\ 1.1010 - 0.000152T & 100°C \leq T \leq 800°C \end{array} \right\}$
	$\beta_{T,\,UPV} = \left\{ \begin{array}{ll} 1 & 23°C \\ 1.0142 - 0.000989T & 100°C \leq T \leq 800°C \end{array} \right\}$
0.2CNF-HSC	$\beta_{T,\,compression} = \left\{ \begin{array}{ll} 1 & 23°C \\ 1.0380 - 0.000900T & 100°C \leq T \leq 800°C \end{array} \right\}$
	$\beta_{T,\,Tensile} = \left\{ \begin{array}{ll} 1 & 23°C \\ 0.9537 - 0.000981T & 100°C \leq T \leq 800°C \end{array} \right\}$
	$\beta_{T,\,Elastic\ Modulus} = \left\{ \begin{array}{ll} 1 & 23°C \\ 0.9978 - 0.00107T & 100°C \leq T \leq 800°C \end{array} \right\}$

	$\beta_{T,\text{Toughness}} = \left\{ \begin{array}{cc} 1 & 23°C \\ 1.322 + 0.001651T & 100°C \le T \le 600°C \end{array} \right\}$
	$\beta_{T,\text{Mass loss}} = \left\{ \begin{array}{cc} 1 & 23°C \\ 1.01027 - 0.00013T & 100°C \le T \le 800°C \end{array} \right\}$
	$\beta_{T,\text{UPV}} = \left\{ \begin{array}{cc} 1 & 23°C \\ 0.9846 - 0.000795T & 100°C \le T \le 800°C \end{array} \right\}$

4.3.17 Mathematical Relationships-BF-HSC

Relationships for properties such as mechanical strength (tensile and compression), associated parameters such as elastic modulus and toughness have been derived. Furthermore, similar relationships for parameters such mass loss of modified formulations that cover the entire exposure range of 23–800ºC are presented. For both the modified formulations (1B-HSC & 2B-HSC), the value of R2 lied in the range of 85% to 97%, which shows good coherence. The relationship between material property degradation and target temperature can be correlated using a coefficient β_T. The values of β_T for elastic modulus, tensile strength, compressive strength, toughness, mass loss are estimated for the modified samples (1B-HSC & 2B-HSC), and are presented in Table 12. At different temperatures, coefficient β_T can be utilized for calculating mechanical properties. These mathematical equations can be helpful to predict performance of BFs reinforced HSC under fire conditions in future analytical studies.

Table 12: Relationship between material property and temperature-BF-HSC

Formulation Type	Property relationships
1B-HSC	$\beta_{T,\text{compression}} = \left\{ \begin{array}{cc} 1 & 23°C \\ 0.9991 - 0.001088T & 100°C \le T \le 800°C \end{array} \right\}$
	$\beta_{T,\text{Tensile}} = \left\{ \begin{array}{cc} 1 & 23°C \\ 0.9987 - 0.001186T & 100°C \le T \le 800°C \end{array} \right\}$
	$\beta_{T,\text{Elastic Modulus}} = \left\{ \begin{array}{cc} 1 & 23°C \\ 0.9939 - 0.00123T & 100°C \le T \le 800°C \end{array} \right\}$
	$\beta_{T,\text{Toughness}} = \left\{ \begin{array}{cc} 1 & 23°C \\ 1.4508 + 0.000913T & 100°C \le T \le 600°C \end{array} \right\}$
	$\beta_{T,\text{Mass loss}} = \left\{ \begin{array}{cc} 1 & 23°C \\ 1.01591 - 0.000167T & 100°C \le T \le 800°C \end{array} \right\}$
2B-HSC	$\beta_{T,\text{compression}} = \left\{ \begin{array}{cc} 1 & 23°C \\ 0.9919 - 0.000985T & 100°C \le T \le 800°C \end{array} \right\}$

	$\beta_{T,\text{Tensile}} = \left\{ \begin{array}{cc} 1 & 23°C \\ 1.0141 - 0.001024T & 100°C \leq T \leq 800°C \end{array} \right\}$
	$\beta_{T,\text{Elastic Modulus}} = \left\{ \begin{array}{cc} 1 & 23°C \\ 1.0071 - 0.001089T & 100°C \leq T \leq 800°C \end{array} \right\}$
	$\beta_{T,\text{Toughness}} = \left\{ \begin{array}{cc} 1 & 23°C \\ 1.6618 + 0.001205T & 100°C \leq T \leq 600°C \end{array} \right\}$
	$\beta_{T,\text{Mass loss}} = \left\{ \begin{array}{cc} 1 & 23°C \\ 1.01429 - 0.000145T & 100°C \leq T \leq 800°C \end{array} \right\}$

CONCLUSIONS AND RECOMMENDATIONS

5.1   Conclusions

Based on the results stipulated in this experimental investigation, the following conclusions are drawn:

1. Visual assessments indicate less physical damage in samples intruded with CNFs compared to control HSC towards higher temperatures ranging in 23-800°C.

2. Visual assessments of formulations modified with BFs exhibit less physical deterioration compared to control HSC in which cracks widen and become observable especially towards higher temperatures

3. The presence of CNFs in concrete matrix enhances the compressive strength both prior to and after fire exposure. This is attributed to the reinforcing action of nanofibers compared to control HSC that spalls off beyond 600°C.

4. The presence of basalt fiber in concrete matrix has an insignificant effect on the compressive strength prior to fire exposure. However, better performance in term of strength retention and physical stability is observed at higher temperatures. Concrete formulations modified with basalt fiber helped to mitigated spalling as compared to control HSC which spalled between 600-800°C.

5. The presence of well dispersed carbon nano fibers in concrete formulations (0.1CNF-HSC and 0.2CNF-HSC) enhances their pre and post fire tension resilience. Beyond critical exposure of 400°C, the CNF based formulations exhibit higher strength retention which is associated with their efficient thermal behavior and crack blunting actions.

6. Concrete reinforced with basalt fibers exhibited enhanced tensile capacity owing to presence of well dispersed basalt fiber. Beyond critical exposure of 400°C, the modified formulations exhibited higher strength retention which is associated with better fire resistance and reinforcing action of basalt fiber.

7. The stress-strain response of CNF-reinforced concretes is relatively less fragile owing higher retention of secant moduli than control concrete in target temperature range of 23-800°C. This is attributed to the preservation of effective load bearing area by crack bridging action of added CNFs.

8. There is a significant difference between stress-strain response of control and modified concrete. The response of basalt fiber concretes is more ductile compared to control HSC which is quantified through toughness index.

9. CNF reinforced concretes suffer with lesser internal structure damage compared to control owing to presence of high-density C-S-H gel, reduced thermal inertia and crack restraining attributes.

10. Higher mass loss is observed in HSC compared to modified concrete formulations which showed better mass retention at elevated temperatures.

11. Simplified high temperature material property relationships have been proposed that can be used as input data in analytical predictions to evaluate elevated temperature response of high strength concrete reinforced with CNFs and BFs.

5.2   Recommendations

- Evaluation of the effect of nano-micro fiber under synergetic mode in SCC, HPC and UHPC mixes with a special focus on spalling behavior.
- Use of SRMs/SCMs alongside these nano-micro fibers and their effect on fire endurance of such matrices.
- Use of CNFs and BFs with other fibers i.e. SF, PP and glass fiber in HSC under elevated temperature conditions

Abbreviations:

HSC	High strength concrete
CNF	Carbon nano fiber
BF	Basalt fiber
UPV	Ultrasonic pulse velocity
SEM	Scanning electron microscopy
PP	Polypropylene fiber
CNTs	Carbon nano tubes
OPC	Ordinary Portland cement
GA	Gum acacia
ASTM	American Society for Testing and Materials
CH	Calcium hydroxide
C-S-H	Calcium silicate hydrate
f_c'	Compressive strength at 28 days
E	Elastic modulus
T_C	Compressive toughness
TI	Toughness indices
β_T	Material Property relationship coefficient

References

1. Khaliq, W. and V. Kodur, *Behavior of high strength fly ash concrete columns under fire conditions.* Materials and Structures, 2012. **46**(5): p. 857-867.
2. Shah, S.N.R., F.W. Akashah, and P. Shafigh, *Performance of High Strength Concrete Subjected to Elevated Temperatures: A Review.* Fire Technology, 2019: p. 121-233.
3. Vardhan, P.R. and T. Muralidhara Rao, *Elevated Temperature and Durability Studies on High Strength Concrete.* CVR Journal of Science & Technology, 2018. **15**(1): p. 10-16.
4. Bangi, M.R. and T. Horiguchi, *Pore pressure development in hybrid fibre-reinforced high strength concrete at elevated temperatures.* Cement and Concrete Research, 2011. **41**(11): p. 1150-1156.
5. Noumowe, A., et al., *High temperature effect on high performance concrete (70-600 C) strength and porosity.* 1994. **145**: p. 157-172.
6. Cheng, F.-P., *stress strain curves for HSC Fu-Ping Cheng1; V. K. R. Kodur.* 2004.
7. Behnood, A. and M. Ghandehari, *Comparison of compressive and splitting tensile strength of high-strength concrete with and without polypropylene fibers heated to high temperatures.* 2009. **44**(8): p. 1015-1022.
8. Phan, L.T. and N.J. Carino, *Review of mechanical properties of HSC at elevated temperature.* 1998. **10**(1): p. 58-65.
9. Agrawal, A. and V. Kodur, *Residual response of fire-damaged high-strength concrete beams.* Fire and Materials, 2019. **43**(3): p. 310-322.
10. Kodur, V., M.S. Dwaikat, and Materials, *Effect of fire induced spalling on the response of reinforced concrete beams.* 2008. **2**(2): p. 71-81.
11. Yong, C. and C.y. Wang, *Thermally induced acoustic emission in Westerly granite.* 1980. **7**(12): p. 1089-1092.
12. Bažant, Z.P., M.F. Kaplan, and Z.P. Bazant, *Concrete at high temperatures: material properties and mathematical models.* 1996.
13. Shah, S., P. Hou, and M. Konsta-Gdoutos, *Nano-modification of cementitious material: Toward a stronger and durable concrete. J Sustain Cem Based Mater 5: 1–22.* 2015.
14. Jeon, I.-Y., et al., *Functionalization of carbon nanotubes*, in *Carbon Nanotubes-Polymer Nanocomposites.* 2011, IntechOpen.
15. Meng, W. and K.H. Khayat, *Mechanical properties of ultra-high-performance concrete enhanced with graphite nanoplatelets and carbon nanofibers.* Composites Part B: Engineering, 2016. **107**: p. 113-122.
16. Gay, C. and F. Sanchez, *Performance of Carbon Nanofiber–Cement Composites with a High-Range Water Reducer.* Transportation Research Record: Journal of the Transportation Research Board, 2010. **2142**(1): p. 109-113.
17. Barbhuiya, S. and P. Chow, *Nanoscaled Mechanical Properties of Cement Composites Reinforced with Carbon Nanofibers.* Materials (Basel), 2017. **10**(6).
18. Konsta-Gdoutos, M.S., et al., *Effect of CNT and CNF loading and count on the corrosion resistance, conductivity and mechanical properties of nanomodified OPC mortars.* Construction and Building Materials, 2017. **147**: p. 48-57.
19. Gao, Y., et al., *Characterization of the interfacial transition zone of CNF-Reinforced cementitious composites.* Cement and Concrete Composites, 2019. **99**: p. 130-139.
20. Lawrence, J.G., L.M. Berhan, and A.J.A.n. Nadarajah, *Elastic properties and morphology of individual carbon nanofibers.* 2008. **2**(6): p. 1230-1236.
21. Mordkovich, V.J., *Carbon nanofibers: a new ultrahigh-strength material for chemical technology.* 2003. **37**(5): p. 429-438.
22. Ozkan, T., M. Naraghi, and I.C. Chasiotis, *Mechanical properties of vapor grown carbon nanofibers.* 2010. **48**(1): p. 239-244.
23. Kang, I., et al., *Introduction to carbon nanotube and nanofiber smart materials.* 2006. **37**(6): p. 382-394.
24. Alrekabi, S., et al., *Mechanical performance of novel cement-based composites prepared with nano-fibres, and hybrid nano- and micro-fibres.* Composite Structures, 2017. **178**: p. 145-156.

25. Lawrence, J.G., L.M. Berhan, and A.R. Nadarajah, *Structural transformation of vapor grown carbon nanofibers studied by HRTEM.* 2008. **10**(7): p. 1155-1167.

26. Sanchez, F. and C. Ince, *Microstructure and macroscopic properties of hybrid carbon nanofiber/silica fume cement composites.* Composites Science and Technology, 2009. **69**(7-8): p. 1310-1318.

27. Singha, K.J. S., *A short review on basalt fiber.* 2012. **1**(4): p. 19-28.

28. Fiore, V., et al., *A review on basalt fibre and its composites.* 2015. **74**: p. 74-94.

29. Irine, F.J. E., *Strength aspects of basalt fiber reinforced concrete.* 2014. **1**(8): p. 192-198.

30. Mingchao, W., et al., *Chemical durability and mechanical properties of alkali-proof basalt fiber and its reinforced epoxy composites.* 2008. **27**(4): p. 393-407.

31. Kizilkanat, A.B., et al., *Mechanical properties and fracture behavior of basalt and glass fiber reinforced concrete: An experimental study.* Construction and Building Materials, 2015. **100**: p. 218-224.

32. Di Ludovico, M., A. Prota, and G.J. Manfredi, *Structural upgrade using basalt fibers for concrete confinement.* 2010. **14**(5): p. 541-552.

33. Sim, J. and C.J. Park, *Characteristics of basalt fiber as a strengthening material for concrete structures.* 2005. **36**(6-7): p. 504-512.

34. Deák, T. and T.Czigány, *Chemical composition and mechanical properties of basalt and glass fibers: A comparison.* 2009. **79**(7): p. 645-651.

35. Lopresto, V., C. Leone, and I.J.C.P.B.E. De Iorio, *Mechanical characterisation of basalt fibre reinforced plastic.* 2011. **42**(4): p. 717-723.

36. Borhan, T.M. Design, *Properties of glass concrete reinforced with short basalt fibre.* 2012. **42**: p. 265-271.

37. Jiang, C.H., et al. *Influence of basalt fiber on performance of cement mortar.* in *Key Engineering Materials*. 2010. Trans Tech Publ.

38. Bazant, Z.P. and M.F. Kaplan, *Concrete at high temperatures: material properties and mathematical models.* 1996: Longman Harlow.

39. Ajayan, P.M, *Nanotubes from carbon.* 1999. **99**(7): p. 1787-1800.

40. Vickers, N.J, *Animal Communication: When I'm Calling You, Will You Answer Too?* 2017. **27**(14): p. R713-R715.

41. Fang, A.W., et al., *Hybrid silicon evanescent devices.* 2007. **10**(7-8): p. 28-35.

42. Adresi, M., *Concrete pavement prediction life model based on electrical response of concrete-CNTs sensors under fatigue loading.* 2019.

43. Parveen, S., S. Rana, and R. Fangueiro, *A Review on Nanomaterial Dispersion, Microstructure, and Mechanical Properties of Carbon Nanotube and Nanofiber Reinforced Cementitious Composites.* Journal of Nanomaterials, 2013. **2013**: p. 1-19.

44. Wang, B., et al., *Effect of highly dispersed carbon nanotubes on the flexural toughness of cement-based composites.* 2013. **46**: p. 8-12.

45. Baloch, W.L., R.A. Khushnood, and W. Khaliq, *Influence of multi-walled carbon nanotubes on the residual performance of concrete exposed to high temperatures.* Construction and Building Materials, 2018. **185**: p. 44-56.

46. Ayub, T., N. Shafiq, and M.F. Nuruddin, *Effect of Chopped Basalt Fibers on the Mechanical Properties and Microstructure of High Performance Fiber Reinforced Concrete.* Advances in Materials Science and Engineering, 2014. **2014**: p. 1-14.

47. Quattrociocchi, G., et al., *Basalt fibres as a sustainable reinforcement for cement based mortars: preliminary study.* 2015. **90**: p. 109-120.

48. Amarkhail, N.J, *Effects of silica fume on properties of high-strength concrete.* 2015. **32**: p. 13-19.

49. Mazloom, M., et al., *Effect of silica fume on mechanical properties of high-strength concrete.* 2004. **26**(4): p. 347-357.

50. 234, A.C. *Guide for the use of silica fume in concrete.* 2006. American Concrete Institute.

51. Khan, M.I., R.J.R. Siddique, Conservation, and Recycling, *Utilization of silica fume in concrete: Review of durability properties.* 2011. **57**: p. 30-35.

52. Lawson, J.R., L.T. Phan, and F. Davis, *Mechanical properties of high performance concrete after exposure to elevated temperatures.* 2000: US Department of Commerce, Technology Administration, National Institute of ….

53. Poon, C.S., et al., *Comparison of the strength and durability performance of normal-and high-strength pozzolanic concretes at elevated temperatures.* 2001. **31**(9): p. 1291-1300.

54. Ergün, A., et al., *The effect of cement dosage on mechanical properties of concrete exposed to high temperatures.* 2013. **55**: p. 160-167.

55. Yüzer, N., et al., *Compressive strength–color change relation in mortars at high temperature.* 2004. **34**(10): p. 1803-1807.

56. Behnood, A., H.J.C. Ziari, and C. Composites, *Effects of silica fume addition and water to cement ratio on the properties of high-strength concrete after exposure to high temperatures.* 2008. **30**(2): p. 106-112.

57. Georgali, B., P.J.C. Tsakiridis, and C. composites, *Microstructure of fire-damaged concrete. A case study.* 2005. **27**(2): p. 255-259.

58. Zhou, Q., F.P.J.C. Glasser, and C. Research, *Thermal stability and decomposition mechanisms of ettringite at 120 C.* 2001. **31**(9): p. 1333-1339.

59. Khoury, G.J.M.o.c.R., *Compressive strength of concrete at high temperatures: a reassessment.* 1992. **44**(161): p. 291-309.

60. Phan, L.T. and N.J. Carino, *Fire performance of high strength concrete: research needs*, in *Advanced Technology in Structural Engineering.* 2000. p. 1-8.

61. Suhaendi, S.L. and T. Horiguchi, *Fiber-Reinforced High-Strength Concrete under Elevated Temperature-Effect of Fibers on Residual Properties.* 2005. **8**: p. 271-278.

62. Khaliq, W., F.J.C. Waheed, and B. Materials, *Mechanical response and spalling sensitivity of air entrained high-strength concrete at elevated temperatures.* 2017. **150**: p. 747-757.

63. Akca, A.H., N. Zihnioğlu, and b. materials, *High performance concrete under elevated temperatures.* 2013. **44**: p. 317-328.

64. Khaliq, W., *Mechanical and physical response of recycled aggregates high-strength concrete at elevated temperatures.* 2018. **96**: p. 203-214.

65. Phan, L.T. and N.J Carino, *Effects of test conditions and mixture proportions on behavior of high-strength concrete exposed to high temperatures.* 2002. **99**(1): p. 54-66.

66. Netinger, I., I. Kesegic, and I.J.F.s.j. Guljas, *The effect of high temperatures on the mechanical properties of concrete made with different types of aggregates.* 2011. **46**(7): p. 425-430.

67. Mehta, P.K. and P.J. Monteiro, *Concrete: microstructure, properties, and materials.* 2006.

68. Khaliq, W. and V.J.A.M.J. Kodur, *Effect of High Temperature on Tensile Strength of Different Types of High-Strength Concrete.* 2011. **108**(4).

69. Tanyildizi, H., A.J.C. Coskun, and B. Materials, *Performance of lightweight concrete with silica fume after high temperature.* 2008. **22**(10): p. 2124-2129.

70. Kodur, V.e., *Properties of concrete at elevated temperatures.* 2014. **2014**.

71. Knaack, A.M., Y.C. Kurama, and D.J.J.A.M.J. Kirkner, *Compressive stress-strain relationships for North American concrete under elevated temperatures.* 2011. **108**(3): p. 270.

72. Pachideh, G. and M. Gholhaki, *An Experimental Study on the Effects of Adding Steel and Polypropylene Fibers to Concrete on Its Resistance after Different Temperatures.* 2018.

73. Cheng, F.-P., V. Kodur, and T.-C.J.J.o.M.i.C.E. Wang, *Stress-strain curves for high strength concrete at elevated temperatures.* 2004. **16**(1): p. 84-90.

74. Xiao, J., et al., *Effect of strain rate on compressive behaviour of high-strength concrete after exposure to elevated temperatures.* 2016. **83**: p. 25-37.

75. Chan, Y., et al., *Residual strength and pore structure of high-strength concrete and normal strength concrete after exposure to high temperatures.* 1999. **21**(1): p. 23-27.

76. Khaliq, W. and V. Kodur, *Effectiveness of Polypropylene and Steel Fibers in Enhancing Fire Resistance of High-Strength Concrete Columns.* Journal of Structural Engineering, 2018. **144**(3).

77. Kodur, V., *Spalling in high strength concrete exposed to fire: concerns, causes, critical parameters and cures*, in *Advanced Technology in Structural Engineering.* 2000. p. 1-9.

78. Bošnjak, J., A. Sharma, and K. Grauf, *Mechanical Properties of Concrete with Steel and Polypropylene Fibres at Elevated Temperatures.* Fibers, 2019. **7**(2).

79. Yu, Z. and D.M. Lau, *Evaluation on mechanical enhancement and fire resistance of carbon nanotube (CNT) reinforced concrete.* 2017. **6**(3): p. 335-349.

80. Antonio, N.J, *Fatigue behavior of steel fibre reinforced concrete.* 1991. **13**(4): p. 239-45.

81. Smarzewski, P., *Study of Toughness and Macro/Micro-Crack Development of Fibre-Reinforced Ultra-High Performance Concrete After Exposure to Elevated Temperature.* Materials (Basel), 2019. **12**(8).

82. Nima, F., A.. Ali, and R. Demirboga. *Development of nanotechnology in high performance concrete.* in *Advanced Materials Research.* 2012. Trans Tech Publ.

83. Metaxa, Z.S., M.S. Konsta-Gdoutos, and S.P. Shah, *Carbon Nanofiber–Reinforced Cement-Based Materials.* Transportation Research Record: Journal of the Transportation Research Board, 2010. **2142**(1): p. 114-118.

84. Zhang, L.W., M.F. Kai, and K.M. Liew, *Evaluation of microstructure and mechanical performance of CNT-reinforced cementitious composites at elevated temperatures.* Composites Part A: Applied Science and Manufacturing, 2017. **95**: p. 286-293.

85. Bastami, M., M. Baghbadrani, and F. Aslani, *Performance of nano-Silica modified high strength concrete at elevated temperatures.* Construction and Building Materials, 2014. **68**: p. 402-408.

86. Lawrence, J.G., L.M. Berhan, and A. Nadarajah, *Structural transformation of vapor grown carbon nanofibers studied by HRTEM.* 2008. **10**(7): p. 1155-1167.

87. Schneider, U., et al., *Recommendation of RILEM TC 200-HTC: Mechanical concrete properties at high temperatures-modelling and applications: Part I. General presentation.* 2007. **40**(9): p. 841-853.

88. RILEM, *129-MHT 'Test methods for mechanical properties of concrete at high temperatures'.* 2004.

89. ASTM, A.J.A.S.f.T. and P. Materials: West Conshohocken, USA, *C150/C150M-17, Standard Specification for Portland Cement.* 2017.

90. Hassani Niaki, M., A. Fereidoon, and M. Ghorbanzadeh Ahangari, *Experimental study on the mechanical and thermal properties of basalt fiber and nanoclay reinforced polymer concrete.* Composite Structures, 2018. **191**: p. 231-238.

91. Tyson, B.M., et al., *Carbon nanotubes and carbon nanofibers for enhancing the mechanical properties of nanocomposite cementitious materials.* 2011. **23**(7): p. 1028-1035.

92. ASTM, C.J.A.C.C.M.-. *Standard test method for compressive strength of cylindrical concrete specimens.* 2012.

93. Xiong, M.-X., J.R Liew, and Design, *Mechanical behaviour of ultra-high strength concrete at elevated temperatures and fire resistance of ultra-high strength concrete filled steel tubes.* 2016. **104**: p. 414-427.

94. Norma, A.J, West Conshohocken, PA, *C496/C496M-11, Standard test method for splitting tensile strength of cylindrical concrete specimens.* 2004: p. 469-90.

95. Concrete, A. Aggregates, *Standard Test Method for Static Modulus of Elasticity and Poisson's Ratio of Concrete in Compression1.* 2014: ASTM International.

96. Heap, M.J., et al., *The influence of thermal-stressing (up to 1000°C) on the physical, mechanical, and chemical properties of siliceous-aggregate, high-strength concrete.* Construction and Building Materials, 2013. **42**: p. 248-265.

97. Castillo, C., *Effect of transient high temperature on high-strength concrete.* 1987, Rice University.

98. Tumadhir M., B., *Thermal and mechanical properties of basalt fibre reinforced concrete.* International Journal of Civil, Environmental, Structural, Construction and Architectural Engineering, 2013. **7**.

99. Kodur, V. and W. Khaliq, *Effect of temperature on thermal properties of different types of high-strength concrete.* 2010. **23**(6): p. 793-801.

100. Phan, L.T., et al., *Effects of elevated temperature exposure on heating characteristics, spalling, and residual properties of high performance concrete.* 2001. **34**(2): p. 83-91.

101. Khaliq, W., H. Khan, and B. Materials, *High temperature material properties of calcium aluminate cement concrete.* 2015. **94**: p. 475-487.
102. Khaliq, W. and F. Waheed, *Mechanical response and spalling sensitivity of air entrained high-strength concrete at elevated temperatures.* Construction and Building Materials, 2017. **150**: p. 747-757.
103. Bonnaud, P.A., Q. Ji, and K. Van Vliet, *Effects of elevated temperature on the structure and properties of calcium–silicate–hydrate gels: the role of confined water.* 2013. **9**(28): p. 6418-6429.
104. Yilmaz, S., Özkan, and V. Günay, *Crystallization kinetics of basalt glass.* 1996. **22**(6): p. 477-481.
105. Fiore, V., et al., *A review on basalt fibre and its composites.* Composites Part B: Engineering, 2015. **74**: p. 74-94.
106. Aseem, A., *Structural Health Assessment of Fire Damaged Building using Non-Destructive Testing and Micro-Graphical Forensic Analysis: A Case Study.* 2019: p. e00258.
107. Neville, A.M. and J.J. Brooks, *Concrete technology.* 1987: Longman Scientific & Technical England.
108. Neville, A.M., *Properties of concrete.* Vol. 4. 1995: Longman London.
109. Yaman, I.O., et al., *Ultrasonic pulse velocity in concrete using direct and indirect transmission.* 2001. **98**(6): p. 450.
110. Arioz, O. and M.A. Journal, *Retained properties of concrete exposed to high temperatures: Size effect.* 2009. **33**(5): p. 211-222.
111. ASTM, USA, *597-83.* 1991.
112. Handoo, S., et al., *Physicochemical, mineralogical, and morphological characteristics of concrete exposed to elevated temperatures.* 2002. **32**(7): p. 1009-1018.
113. Baloch, W.L., et al., *Effect of Elevated Temperatures on Mechanical Performance of Normal and Lightweight Concretes Reinforced with Carbon Nanotubes.* Fire Technology, 2018. **54**(5): p. 1331-1367.
114. Minitab. *https://www.minitab.com/en-us/products/minitab/*. 2017.